Journal of Molecular Structure 1344 (2025) 143011

Contents lists available at ScienceDirect

Journal of Molecular Structure

journal homepage: www.elsevier.com/locate/molstr

Synthesis, single crystal XRD, DFT, molecular docking studies and antioxidant capacity and antibacterial evaluation of β -phenylethylamine derivative schiff base compound

Kübra Öztürk [a,*], Ebrar Nur Özkan [b], Çiğdem Er Çalışkan [c], Sertan Aytaç [d], Özlem Gündoğdu Aytaç [d]

[a] Kırşehir Ahi Evran University, Department of Genetics and Bioengineering, Faculty of Engineering and Architecture, Kırşehir, Türkiye
[b] Atatürk University, Faculty of Science, Department of Chemistry, Erzurum, Türkiye
[c] Kırşehir Ahi Evran University, Department of Field Crops, Faculty of Agriculture, Kırşehir, Türkiye
[d] Kırşehir Ahi Evran University, Kaman Vocational School, Department of Food Technology, Kırşehir, Türkiye

ARTICLE INFO

Key words:
Single Crystal XRD
DFT
Molecular docking
Antioxidant
Antibacterial

ABSTRACT

In this study, (*E*)-5-(((4-(dimethylamino)phenyl)imino)methyl)-2-methoxyphenol (**K2**) was synthesized and characterized. Its structure was determined by single crystal X-ray diffraction and was shown to belong to the monoclinic C2/c space group. By Hirshfeld surface analysis, the most dominant intermolecular interactions were found to be H···· H (%54,5), H···· C/C··· H (%25,2) and H···· O/O··· H (%12,4). The total surface area was calculated as 320.95 Å^2. The geometry and reactivity of the molecule were investigated by DFT calculations (B3LYP/631G(d,p)). HOMO and LUMO energy values were determined as -0.2820 eV and -0.11707 eV, respectively, and the energy gap was found as ΔEgap = 0.164 eV. Also, the polarizability was found as 399.94 a. u. and the dipole moment as 4.65 Debye. These theoretical calculations show that **K2** can be easily polarized under an electric field and has a permanent dipole moment. Additionally, the antimicrobial and antioxidant properties of the compound were studied. It was found to be effective against Gram-positive and Gram-negative bacteria at a level comparable to Gentamicin and Ciprofloxacin. Furthermore, molecular docking simulations were performed to investigate the interaction of **K2** with biologically important proteins (1NHJ, 3QX3, 2XO8 and 1HD2). **K2** showed the strongest interaction with Human Peroxiredoxin 5 (1HD2) with a binding energy of -7.45 kcal/mol, suggesting that it may have antioxidant properties and may be a potential therapeutic candidate for oxidative stress-related diseases.

Introduction

Nitrogen-containing compounds are widely used in drug development studies due to their structural diversity and broad pharmacological activities [1]. Dopamine and β-phenylethylamine are also among the important nitrogen-containing compounds. In particular, dopamine (3, 4-dihydroxyphenethylamine) is a β-phenylethylamine derivative that plays a crucial role in neurological functions (Fig. 1) [2].

Imbalances in dopamine levels can lead to various diseases such as Parkinson's disease (PD), Alzheimer's disease (AD), attention deficit hyperactivity disorder (ADHD), and restless leg syndrome [3,4]. The treatment of these diseases involves the use of dopamine-like drugs (Selegiline, Safinamide) or monoamine oxidase enzyme inhibitors (MAO) (Clorgyline, Lazabemide) [5] (Fig. 2).

β-Phenylethylamine is a compound belonging to the natural monoamine alkaloid class, produced by various plants, algae, fungi, and bacteria [6]. This compound, which functions as a neuromodulator or neurotransmitter in the mammalian central nervous system [7], exhibits various pharmacological properties such as neuropsychiatric, antidepressant, stimulant, bronchodilator, and decongestant effects through its derivatives [8].

Nitrogen-containing heterocyclic groups or amine functional groups are present in the structure of many drugs with biological properties such as anticancer, antimicrobial, analgesic, and anti-inflammatory effects [1,9]. Schiff bases, which belong to these compounds, possess an imin (HC═*N*) functional group and exhibit various biological activity

* Correspondence author.
E-mail address: kubra.ozturk@ahievran.edu.tr (K. Öztürk).

https://doi.org/10.1016/j.molstruc.2025.143011
Received 5 May 2025; Received in revised form 4 June 2025; Accepted 16 June 2025
Available online 16 June 2025

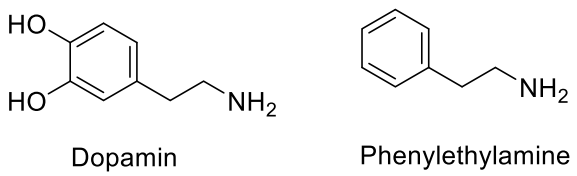

Fig. 1. Chemical structures of β-phenylethylamine and dopamine.

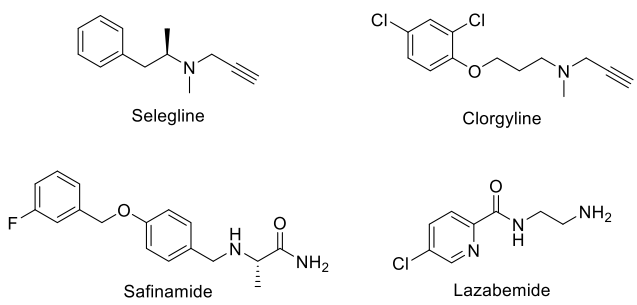

Fig. 2. Commercially available dopamine-like drugs.

properties [10,11]. Schiff bases have different chemical and biological interactions due to the sp^2 hybridized nitrogen atom in the pharmacophore group and the unshared electron pair it has [12]. These compounds, offering a wide range of biological activities such as antiviral, antibacterial, biocidal, enzymatic reaction inhibition, and plant growth regulation, have gained significant interest in the pharmaceutical field [13,14].

In recent years, various Schiff bases containing N, O, S and P atoms have been evaluated as potential drugs and drug candidates in the pharmaceutical industry [15], and have also found widespread use in different industrial areas such as polymer, cosmetics, electronic materials, textile dye production and liquid crystal technology [16–18]. However, traditional synthesis methods of Schiff bases have various disadvantages such as low yield, harsh reaction conditions, long reaction times and high catalyst requirement. Many new synthesis methods have been developed in the last two decades to overcome these limitations. In particular, the microwave technique, which reduces by-product formation in organic syntheses, shortens the reaction time and provides high yield, stands out as an important alternative that enables more efficient production of Schiff bases [19].

Schiff bases are of great interest not only for their biological activities but also for theoretical studies. Density functional theory (DFT) calculations help determine the relationship between the molecular structures and properties of compounds [20]. Quantum mechanical calculations allow us to better understand the electronic structure and interactions of molecules [21]. DFT, one of the most successful theories in determining the fundamental properties of matter, offers many important applications such as modeling the band structure of solids and calculating bond energies [22].

Hirshfeld surface analysis is used as an important graphical tool for more detailed analysis of intermolecular interactions. This technique provides qualitative and quantitative data by visualizing the contacts between molecules in the crystal structure [23]. When used together with DFT calculations, more in-depth information about the stability and interaction mechanisms of molecular systems can be obtained.

The development and introduction of pharmaceuticals is a long and costly process. In this process, molecular docking studies are a widely used computational approach to examine protein-ligand interactions and identify potential drug candidates. Thanks to this method, which is a critical step in structure-based drug design, the effectiveness of candidate molecules against diseases can be predicted in a short time, providing advantages in terms of both time and cost [24].

Especially in the fight against infectious diseases, the discovery of new and effective compounds is of great importance. Factors such as the increase in drug resistance, side effects of existing antibiotics and the re-emergence of infections increase the need for new antimicrobial agents against infectious diseases, which are a significant public health problem worldwide. In this study, β-phenylethylamine and vanillin were selected as starting compounds and a new Schiff base was synthesized with the help of microwave energy. The antimicrobial and antioxidant properties of the synthesized compound were examined and its crystal structure was confirmed by XRD technique. In addition, theoretical studies of the compound were carried out with DFT calculations (Gaussian 16) and molecular docking studies (AutoDock Tools) and the results obtained were reported.

Experimental

Materials and methods

Chemicals were purchased from various companies and used directly without any purification. Bruker 400 MHz NMR spectrometer (^{1}H NMR 400 MHz, ^{13}CNMR 100 MHz) was used for NMR analyses. Melting points of the products were determined with a GallenKamp MPD 350 capillary melting point device. Reactions were performed via Vestel MD 20 DB model microwave oven (230 V-50 Hz, 900 W). HR-MS: electron spray technique (*M*+/M-) from the soln. in MeOH (Waters LCT Premier TM XE UPLC/MS TOF (Manchester, UK)

Acetylcholinesterase, acetylcholine iodide2,2′-azino-bis 3-ethylbenzthiazoline-6-sulfonic acid ($ABTS^{\bullet+}$), 1,1-diphenyl-2-picrylhydrazyl (DPPH), 2,9-dimethyl-1,10-phenanthroline (Neocuproine), trolox, solvents were obtained from Sigma-Aldrich. They were analytical grade and used without further purification steps.

General procedure for the synthesis of Schiff base

Schiff base **K2** was synthesized as described according to the procedures, which given in literature [14,19]. Phenylethylamine (**1**) (1 mmol) was added to 3-hydroxy-4-methoxybenzaldehyde (**2**) (1 mmol) (Scheme 1). Then, the reaction mixtures were exposed to microwave radiation at 900 W and was monitored by TLC. Compounds was purified by crystallization (MeOH/P.Ether). This compound **K2** with (E)-configuration were observed that a single product formed according to ^{1}H NMR and ^{13}C NMR spectrum results and X-Ray analysed.

(*E*)-5-(((4-(dimethylamino)phenyl)imino)methyl)-2-methoxyphenol **(K2) :** It was obtained in a 97 % yield as a colourless crystal. m.p:70.3 °C. ^{1}H NMR (400 MHz, $CDCl_3$) δ 8.06 (s, 1H), 7.32 - 7.20 (m, 7H), 6.88 (d, J = 8.3 Hz, 1H), 3.93 (s, 3H), 3.86 (dd, J = 15.6, 8.2 Hz, 2H), 3.02 (t, J = 7.5 Hz, 2H). ^{13}C NMR (100 MHz, $CDCl_3$) δ 161.12, 148.93, 145.92, 140.01, 129.86, 129.06, 128.33, 126.08, 121.13, 113.60, 110.32, 63.02, 55.94, 37.58. HRMS: (ESI), *m/z*: [M^+H] + Calcd for $C_{16}H_{17}NO_2$ 256.1259; found 256.1334.

Crystal structure determination

For the crystal structure determination, single-crystal of the $C_{32}H_{34}N_2O_4$ molecule was used for data collection on a Bruker APEX-II CCD diffractometer. Graphite-monochromated Mo-Kα radiation (λ = 0.71073 Å) and oscillation scans technique with $\Delta w = 5^\circ$ for one image were used for data collection. The lattice parameters were determined by the least-squares methods on the basis of all reflections with $F^2 > 2\sigma(F^2)$. Integration of the intensities, correction for Lorentz and polarization effects and cell refinement was performed using CrystalClear (Rigaku/MSC Inc., 2005) software. The crystal structures were solved by direct methods using SHELXS-2013**,** which enabled the identification of most of the heavier atoms. The remaining non-hydrogen atoms were subsequently located from difference Fourier maps generated through successive full-matrix least-squares refinement cycles based on F^2, carried out with SHELXL-2013 [25]. All non-hydrogen atoms were refined

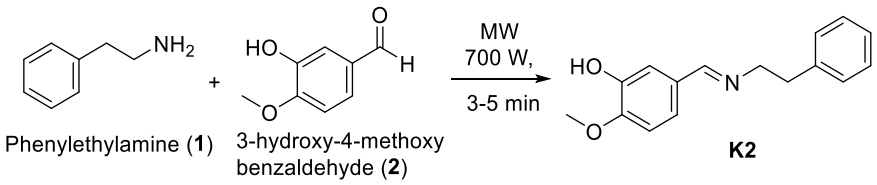

Scheme 1. Microwave assisted synthesis of Schiff base **K2.**

using anisotropic displacement parameters. The hydrogen atoms were assigned with common isotropic displacement factors and included in the final refinement by using geometrical restrains. The final difference Fourier maps showed no peaks of chemical significance. Crystal data for crystal: $C_{32}H_{34}N_2O_4$, crystal system, space group: monoclinic, C2/c; (no:12); unit cell dimensions: $a = 27.794(2)$, $b = 5.5186(4)$, $c = 17.8651(15)$ Å, $\alpha = 90$, $\beta = 96.341(3)$, $\gamma = 90°$; volume; 2723.5(4) Å^3, $Z = 4$; calculated density: 1.245 g/cm^3; absorption coefficient: 0.082 mm^{-1}; F (000): 1088.0; θ-range for data collection 5.174–56.628°; refinement method: full matrix least-square on F^2; data/parameters: 3378/177; goodness-of-fit on F^2: 1.040; Data completeness; 1.00, final R-indices [$I > 2\,\sigma$ (I)]: R1 = 0.048, wR2 = 0.117; largest diff. peak and hole: 0.21 and −0.17 eÅ^{-3}.

CCDC- 2441,556 contains supplementary crystallographic data. These data are provided free of charge via the joint CCDC/FIZ Karlsruhe deposition service www.ccdc.cam.ac.uk/structures.

X-ray data collection and structure refinement

Single crystals of $C_{32}H_{34}N_2O_4$ **K2** were selected and mounted on a Bruker APEX-II CCD diffractometer. The crystal was kept at 273.15 K during data collection. Using Olex2 [26], the structure was solved with the olex2.solve [27] structure solution program using Charge Flipping and refined with the SHELXL [28] refinement package using Least Squares minimization.

Mercury programs were employed for drawing. The hydrogen atoms of CH and OH were found in a difference Fourier map and refined isotropically. The positions of other hydrogen atoms were calculated at the distances of 0.93 Å, 0.97 Å, and 0.96 Å for aromatic CH, CH_2 and CH_3 respectively. A riding model was used for refinement by applying the constraints of $U_{iso}(H) = k$ X Ueq (C) (Table 1).

Table 1
Crystallographic data and refinement parameters for the title compound.

Empirical formula	$C_{32}H_{34}N_2O_4$
Formula weight	510.61
Temperature/K	273.15
Crystal system	monoclinic
Space group	C2/c
a/Å	27.794(2)
b/Å	5.5186(4)
c/Å	17.8651(15)
α/°	90
β/°	96.341(3)
γ/°	90
Volume/Å^3	2723.5(4)
Z	4
ρ_{calc}g/cm^3	1.245
μ/mm^{-1}	0.082
F (000)	1088.0
Crystal size/mm^3	0.15 × 0.13 × 0.12
Radiation MoK$_\alpha$	(λ = 0.71073)
2Θ range for data collection/°	5.174 to 56.628
Index ranges	$-36 \le h \le 36$, $-7 \le k \le 7$, $-23 \le l \le 23$
Reflections collected	28,974
Independent reflections	3378 [R_{int}= 0.0357, R_{sigma} = 0.0234]
Data/restraints/parameters	3378/0/177
Goodness-of-fit on F^2	1.005
Final R indexes [$I \ge 2\sigma$ (I)]	R1 = 0.0481, wR2 = 0.1193
Final R indexes [all data]	R1= 0.0658, wR2 = 0.1282
Largest diff. peak/hole / e Å^{-3}	0.208/−0.17

Crystallographic data has been submitted to the Cambridge crystallographic center under the CCDC deposition number 2441556. Copies of the data can be obtained through application to CCDC, 12 Union Road, Cambridge CB2 1EZ, UK. (fax: +44 1223 336033 or e-mail: deposit@ccdc. cam.ac.uk or at http://www.ccdc.cam.ac.uk). X-ray experimental details are given in Table 7 below.cif structure file and checkcif report has been attached.

Reducing ability assays

The absorbance of Cu^{2+} reducing ability of Schiff base (**K2**) was determined according to our previous study [29]. For this purpose, 0.25 mL $CuCl_2$ solution (10 mM), 0.25 mL ethanolic neocuproine solution (7.5×10^{-3} M) and 250 μL NH_4Ac buffer solution (1.0 M) in different concentrations (25–500 μg/mL) were transferred to test tubes containing Schiff base (**K2**) sample. After diluting the total volume to 2 mL with distilled water and incubating for 30 min, the absorbance of the solution was measured at 450 nm. The reducing effects of the compounds and the standard were recorded spectrophotometrically based on these absorbance values.

For the Fe^{3+} reduction test, various concentrations of the compounds were transferred into test tubes, followed by the addition of 2.5 mL of phosphate buffer (0.2 M, pH 6.6) and 2.5 mL (1 %) of potassium ferricyanide [$K_3Fe(CN)_6$] solutions. The mixture was vortexed and incubated at 50 °C for 20 min. Then 2.5 mL of trichloroacetic acid (10 %) was added and the top layer was mixed with 2.5 mL of distilled water and 0.5 mL of $FeCl_3$ (0.1 %). The reducing effects of the compounds and the standard were recorded spectrophotometrically at 700 nm absorbance values [24].

Radical scavenging capacities

DPPH• · and $ABTS^{\bullet+}$ scavenging methods are the most widely used spectrophotometric methods to determine the antioxidant capacity of newly synthesized compounds. DPPH• · scavenging effect of Schiff base (**K2**) was realized according to Blois method [30]. Briefly, 1 mL of DPPH• • solution (0.1 mM), which was prepared in ethanol and possessed violet / purple color depending on the concentration of the antioxidant, was added to the Schiff base (**K2**) samples at different concentrations (25–500 μg/mL). Then, they were incubated at room temperature for 30 min and their absorbance values were recorded at 517 nm. In the $ABTS^{\bullet+}$ radical cation scavenging assay to calculate antioxidant capacity based on this radical scavenging ability. Firstly, aqueous solution of $ABTS^{\bullet+}$ (7.0 mM) is oxidized by oxidants like $K_2S_2O_8$ (2.5 mM) for production of its radical cation ($ABTS^{\bullet+}$) [31]. The $ABTS^{\bullet+}$ solution was diluted with a phosphate buffer (0.1 M, pH 7.4) prior to use, adjusting the absorbance value of the control to 0.750 ±0.025 at 734 nm. Then, 1 mL of $ABTS^{\bullet+}$ solution was added 3 mL of Schiff base (**K2**) solution at different concentrations. After 30 min the remaining absorbance of $ABTS^{\bullet+}$ measured at 734 nm. IC_{50} values were calculated using the dose-response curves obtained.

Antimicrobial activity testing

The antimicrobial activities of the synthesized compound **K2** were determined by agar well diffusion method recommended by the National Committee for Clinical Laboratory Standards (NCCLS 2000).

The antimicrobial effect of this compound was tested against pathogenic microorganisms such as *Staphylococcus aureus* (ATCC 25213), *Bacillus cereus* (709 Roma), *Enterococcus faecalis* (ATCC 29212), *Listeria monocytogenes* (ATCC 43251), *Acinetobacter baumannii* (ATCC 02026), *Klebsiella pneumoniae* (ATCC 10031), *Escherichia coli* (ATCC 25922), and *Pseudomonas aeruginosa* (ATCC 43288). Stock solutions of the molecules were prepared in 10 % dimethyl sulfoxide (DMSO) at a concentration of 10 mg/mL. The microorganisms used in the experiment were incubated in a nutrient medium for 24 h at 37 °C. Each microorganism was suspended in sterile sailing and adjusted to a concentration of 1×10^6 CFU/mL. Wells of the culture plates were punched with 6 mm diameter holes using a sterile cork drill and inoculated completely with bacterial suspensions. In the final step, the petri dishes were placed in an incubator at 37 °C for 24 h. At the end of the incubation period, the diameter of the zone of inhibition (mm) formed by each test compound against bacterial growth was measured using the antibiogram zone measurement scale. Ampicillin and cycloheximide were used as positive controls and 10 % DMSO were used as negative control.

Computational investigations

Density functional theory (DFTs) studies

DFT-based computations are emerging as an important approach in theoretical medicinal chemistry. The basic assumption of DFT (Density Functional Theory) is that the electronic density of a system only determines the ground state energy and other atomic properties of the system [32]. DFT (Density Functional Theory) has proven its effectiveness in the analysis of medicinal molecule geometries by successfully predicting the geometries of smaller organic compounds. The agreement between theoretical calculations and experimental data performed with DFT has been supported by numerous studies demonstrating the applicability of this technique. In this context, DFT stands out as a useful tool in the study of electron affinities, ionization energies, relative energies and metal-ligand bond strengths Tandon, 2019. In our study, B3LYP/6–31G(d,p) level of theory was used to perform DFT calculations. B3LYP is one of the most preferred hybrid functionals and is known for its cost-effectiveness and accuracy. The B3LYP/6–31 G (d,p) basis set was used to optimize the geometry of the synthesized compound **K2**. In addition to physical parameters, global reactivity descriptors of the synthesized compound **K2** were assessed. Gaussian 09 [33] software was used to carry out DFT calculations on multi-core systems, and Gauss View 6 [https://gaussian.com/wp-content/uploads/dl/gv6.pdf] were used to visualize optimized structures.

Molecular docking

Molecular docking analysis

Molecular docking studies play a crucial role in drug design and pharmacology, providing insights into protein-ligand interactions and potential binding sites efficiently. This method is widely regarded as a reliable and rapid tool for screening molecular interactions, making it valuable for early-stage drug discovery [34]. In our study, in silico molecular docking interactions of compound **K2** with selected proteins were analyzed using AutoDock Tools. Crystal structure of N-terminal 40KD MutL/A100P mutant protein complex with ADPnP and one sodium (PDB: 1NHJ) [35], Human topoisomerase-II beta in complex with DNA and etoposide (PDB: 3QX3) [36] cytochrome c peroxidase: ascorbate bound to the engineered ascorbate binding site (PDB: 2X08), [37], Human peroxiredoxin 5 (antioxidant receptor) (PDB: 1HD2) [38] was retrieved from the protein database (https://www.rcsb.org/).

The PDB: **1NHJ** structure provides important contributions to the understanding of how the **MutL** protein, one of the key components of the DNA mismatch repair (MMR) system, functions at the molecular level by revealing its structure. This structure plays a critical role in many areas such as elucidating the molecular basis of diseases, developing new generation cancer treatments, infectious diseases, and designing drugs targeting DNA repair pathways [39].

The PDB: **3QX3** structure belongs to the human DNA topoisomerase II beta (TOP2B) enzyme and presents the three-dimensional conformation of the enzyme in complex with DNA. TOP2B plays an important role in basic cellular processes such as replication and transcription by regulating the superhelical structure of DNA [40,41]. This structure is important in terms of evaluating the potential interactions of antibiotics with human topoisomerases. DNA topoisomerases are important therapeutic targets for both anticancer and antibacterial drugs [42–44]. In this direction, TOP2B is widely used in the investigation of the inhibitory potential of antimicrobial and antitumor agents at the molecular level [45,46].

Among the most dangerous species for the human body and living organisms in general are reactive oxygen species (ROS) naturally produced in the human body. However, excessive production of ROS endangers the human body in various ways and can lead to serious biological damage. Vitamin C (ascorbic acid) exhibits important inhibitory properties in minimizing the harmful effects of ROS both in the human body and in microorganisms such as *Streptococcus pneumoniae* and *Saccharomyces cerevisiae* [37]. Cytochrome c peroxidase (CCP) is a heme-containing, water-soluble enzyme. It provides protection against oxidative stress by neutralizing harmful reactive oxygen species, especially hydrogen peroxide, in the cell. It also acts as a sensor that activates mitochondrial catalase and plays an important role in electron transfer between proteins [47,48]. In this study, in vitro antioxidant activity and in silico docking studies were carried out against cytochrome c peroxidase enzyme (PDB code: 2X08) in order to evaluate the suitability of the synthesized compound as a potential antioxidant and to validate its activity at theoretical level [49,50].

PDB 1HD2 structure, human Peroxiredoxin 5 (PRDX5), an antioxidant enzyme found in humans, protects cells against oxidative stress. The structural information of this enzyme is available in the Protein Data Bank. Peroxiredoxins are a family of peroxidases that reduce hydrogen peroxide and alkyl hydroperoxides using reducing equivalents derived from thiol-containing donor molecules. These donor molecules include thioredoxin, glutathione, trypanothione, and AhpF. PRDX5 is a novel mammalian thioredoxin peroxidase species that is widely expressed in tissues and localized to different cellular regions such as mitochondria, peroxisomes, and cytosol. Functionally, PRDX5 plays an important role in antioxidant defense mechanisms and signal transduction processes in cells [51].

The protein preparation was performed following the standard protocol [36,52]. This process involved removing the co-crystallized ligand, selected water molecules, and cofactors. The target protein file was prepared by retaining the associated residues using the AutoDock 4.2 (MGL Tools 1.5.7) automatic preparation function. Before docking, the molecule (**K2**) and the ligand were optimized using Avogadro, a molecular modeling software. This step ensured that their structures were correctly determined and minimized. The optimized structures were then saved in PDB format for subsequent docking studies. The proteins and ligands were prepared using MGLTools, which included the removal of water molecules and the addition of polar hydrogen atoms and charges. Torsion angles were verified, and Kollman charges were added to ensure accurate docking. The final structures were re-saved in PDB format. The active sites of the proteins were identified, and grid box parameters were carefully set to **60×60×60 Å³** with a spacing of **0.553 Å**. 27.806, 8.509, 31.764 x, y, z centers for N-terminal 40KD MutL/A100P mutant protein complex with ADPnP and one sodium (PDB: 1NHJ), 33.995, 95.778, 50.768 x, y, z centers for Human topoisomerase-II beta in complex with DNA and etoposide (PDB: 3QX3), 67.793, 48.847, −46.031 x, y, z centers for cytochrome c peroxidase: ascorbate bound to the engineered ascorbate binding site (PDB: 2X08) and 14.472, 35.908, 18.287 x, y, z centers for Human peroxiredoxin 5 (antioxidant receptor) (PDB: 1HD2). The prepared files were then converted into PDBQT format using Discovery Studio Visualizer 4.0 for docking. The docking process utilized the Lamarckian Genetic

Algorithm (LGA), a widely used method for molecular docking. This algorithm efficiently predicted interactions between the protein and ligand, including Van der Waals forces, polar contacts, and other non-covalent interactions. By automating the calculation of these interactions, the study provided insights into the binding affinities and interaction patterns between the selected receptor and the ligands. Molecular docking scores that provide insights into binding affinity and interaction strength are presented in Fig. 10–13. These scores reflect how well ligands fit into the active sites of target receptors and the predicted strength of ligand-receptor interactions.

Result and discussion

Chemistry

Schiff base (**K2**) was synthesized by reacting phenylethylamine (**1**) with 3-hydroxy-4-methoxybenzaldehyde (**2**) in a 1:1 molar ratio. The reaction was carried out under microwave irradiation, yielding the target compound with a high efficiency. Structural characterization was carried out using ^{1}H and ^{13}C NMR spectroscopy, recorded in $CDCl_3$ on a 400 MHz (^{1}H) / 100 MHz (^{13}C) Varian spectrometer.

In the ^{1}H NMR spectrum, the imine proton appeared as a singlet at 8.06 ppm. Aromatic protons were determined as multiplets in the range of 7.32–7.20 ppm and as doublets at 6.88 ppm. In the ^{13}C NMR spectrum, the imine carbon typically gave a signal at 161.12 ppm. Further confirmation of the proposed molecular structure was provided by mass spectrometry (MS), with the results being in full agreement with the expected structure.

X-Ray structure

Single-crystal X-ray diffraction analysis has revealed that the **K2** molecule consists of a substituted (methoxy and hydroxyl) benzene ring and an unsubstituted benzene ring, linked by a nitrogen (N1)-containing bridging chain (Fig. 3). The bond length between the C8 and N1 atoms in the bridging chain was determined to be 1.2677 (18) Å. This value is significantly shorter than the typical C—N single bond lengths observed in aliphatic amines (approximately 1.43–1.47 Å; [53] Conversely, this bond length aligns well with the range of C=N double bond lengths commonly found in imines and similar nitrogen-containing double bond systems (1.27-1.30 Å) [54,55]. Data from the Cambridge Structural Database (CSD) also supports similar C=N bond lengths (CSD, query: "C=N double bond", imine). Therefore, the obtained bond length strongly indicates the presence of significant double bond character between the C8 and N1 atoms. This double bond character may arise from the interaction of the lone pair of electrons on the nitrogen atom with a neighboring π system, and it can also contribute to the molecule adopting a specific conformation by restricting rotation within the bridging chain. Furthermore, this structural feature is expected to influence the molecule's chemical reactivity and other physicochemical properties.

K2 molecules form a regular three-dimensional network within a monoclinic crystal system. Unit cells repeat to create an extended structure. Molecules appear stacked in layers, and intermolecular hydrogen bonds significantly influence the packing arrangement and crystal stability. Dense packing supports the absence of solvent molecules, and the repeating molecular pattern reflects the C2/c space group symmetry. This arrangement is important for understanding the material's macroscopic properties.

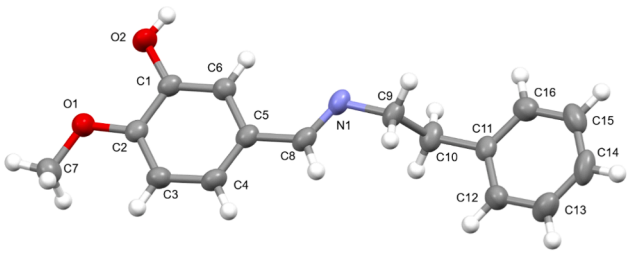

Fig. 3. X-ray structure of the molecule **K2**. Thermal ellipsoids are drawn at the 50 % probability level.

The molecules in the crystal structure are packed in a regular three-dimensional lattice, as illustrated in Fig. 4. The unit cell, delineated by a black rectangle in Fig. 4, clearly shows that the molecules are stacked in specific orientations and potential layers. In this ordered packing arrangement, strong intermolecular O—H···N and N—H···O hydrogen bonds with a length of 2.848 Å, detailed in Fig. 4, are considered to play a significant role. These hydrogen bonds effectively link neighboring molecules, contributing to the formation of a stable three-dimensional network and causing the molecules to be fixed in specific geometric positions.

Careful examination of the overall packing arrangement in Fig. 4 reveals the presence of some void regions. However, previous analyses have not provided any evidence for the presence of solvent molecules within these voids. The obtained crystal structure definitively demonstrates the existence of strong intermolecular hydrogen bonds between the molecules. These O—H···N and N—H···O hydrogen bonds (Fig. 4), measuring 2.848 Å, form the foundation of the crystal lattice and guide the highly ordered packing of the molecules. The directional nature of these hydrogen bonds is of critical importance in the formation of the potential layered structure observed in Fig. 4. The stacking of molecules along specific planes can also be supported by other weaker interactions such as van der Waals forces and possible π-π stacking interactions between the layers.

The void regions observed in the crystal packing theoretically have the potential to allow for porosity and the uptake of guest molecules into the crystal structure. However, in this study, no significant electron density was detected within these voids, suggesting that they are largely empty. Nevertheless, the size and shape of these voids may present interesting research topics for future investigations regarding the crystal's potential applications. Furthermore, an intramolecular H···H contact within the molecule may indicate internal steric strain, which could influence the molecule's preferred conformation.

In general, the lengths of hydrogen bonds vary depending on several factors, including the electronegativity and geometry of the donor and acceptor atoms, as well as environmental factors. However, the typical length ranges reported in the literature for O···N and N···O hydrogen bonds are as follows: O···N hydrogen bonds typically range from 2.6 Å to 3.2 Å, with strong O—H···N bonds being shorter (2.6–2.8 Å) and weaker ones extending up to 3.0 Å. Similarly, N···O hydrogen bonds also generally fall within a range of 2.7 Å to 3.3 Å, with strong N—H···O bonds being shorter (2.7–2.9 Å). The hydrogen bonds identified in this study, with a length of 2.848 Å (Table 2), fall within the typical O···N and N···O hydrogen bond length ranges reported in the literature by Desiraju & Steiner (1999) and Jeffrey (1997) [56,57]. This clearly indicates that these interactions are strong and structurally significant.

In conclusion, the crystal structure of the **K2** compound exhibits a highly ordered three-dimensional packing driven by strong hydrogen bonds. These fundamental structural features provide valuable insights for understanding the solid-state behavior and potential application areas of the compound.

The potential C—H···π interaction highlighted by PLATON offers an important point for understanding the crystal structure of **K2**. The distance of 2.78 Å between the -H hydrogen atom and the centroid of the aromatic ring suggests that such an interaction is geometrically possible. C—H···π interactions are composed of components such as electrostatic attraction, dispersion forces, and a limited degree of charge transfer, and they are positioned somewhere between hydrogen bonds and van der Waals interactions on the spectrum of intermolecular interactions. C—H···π interactions arise from the interaction of a hydrogen atom (δ+) of a CH group with a π-electron system (typically an aromatic ring).

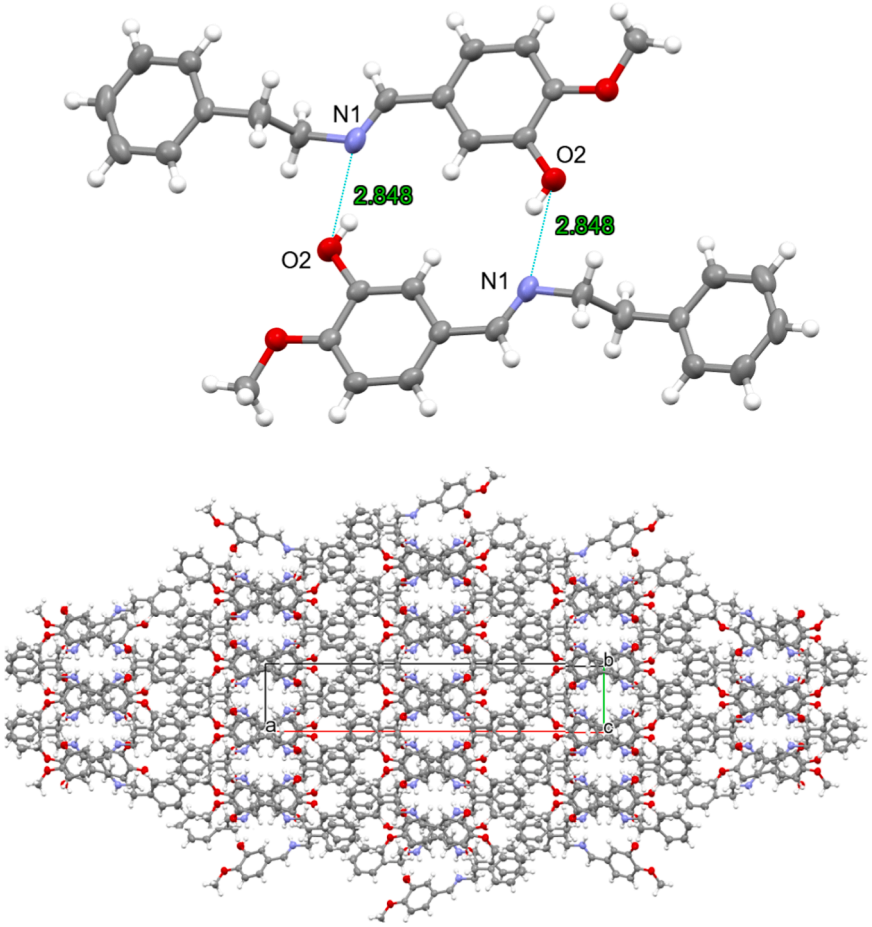

Fig. 4. The unit cell packing of the title compound viewed along the *a-axis*.

Table 2
Hydrogen bond geometry (Å, °).

D–H···A	D–H	H···A	*D*···A	D–H···A
O2–H2O···N^{i}	0.82	2.13	2.8480 (15)	146

Symmetry code; i: -x,1-y,-z; ii : x,1 + *y*,z; iii : 1/2 + *x*,3/2-y,1/2 + *z*.

Although these interactions are not as strong as hydrogen bonds, they can play a significant role in molecular recognition and the stability of crystal packing [58].

The observed H···Cg (centroid) distance of 2.78 Å falls within the range of typical C—H···π interaction distances reported in the literature [59]. This suggests that this interaction could be a weak but directional force contributing to the crystal packing.

This potential C—H···π interaction may help in positioning the molecules relative to each other in a specific geometry, thereby contributing to the formation of the observed crystal lattice. In particular, such interactions between aromatic rings can influence the stacking arrangement and layering of molecules (Fig. 4).

The presence of this potential interaction indicates that not only hydrogen bonds but also weaker but directional interactions play a role in the crystal packing. In particular, the π-electron systems of aromatic rings can interact with CH groups of neighboring molecules, contributing to the specific alignment and stacking of molecules. Upon examining the packing arrangement in Fig. 4, it can be considered that such interactions in regions where aromatic rings are positioned close to each other may help to stabilize the crystal lattice by optimizing intermolecular distances and orientations.

C—H···π interactions hold a significant place in crystal engineering. These interactions can be utilized to predict and control the packing arrangement of molecular crystals. For example, aromatic rings and suitable CH donor groups can be incorporated into the molecular structure to achieve a specific packing motif. In this context, the potential interaction observed in K2 provides a valuable clue for understanding the crystallization behavior of the molecule and the resulting solid-state structure.

However, the strength of C—H···π interactions depends on various factors, including the H···Cg distance, as well as the orientation of the CH bond (H—C···Cg (centroid) angle) and the nature of the aromatic ring. The H—C···Cg (centroid) angle reported in the PLATON analysis, with a very small value of 2.6 degrees, indicates that the geometry of the potential C—H···π interaction deviates significantly from the ideal. As mentioned in the literature, the H—C···Cg (centroid) angle in typical and effective C—H···π interactions is usually in the range of 150–180 degrees [57,58]. C—H···π interactions in molecular crystals [57]. This small angle (2.6 degrees) suggests that the hydrogen atom is not interacting with the π system in a favorable orientation. In this case, despite the reported H···Cg(centroid) distance of 2.78 Å, the H—C···Cg angle of 2.6 degrees indicates that this interaction is non-linear and therefore very weak or negligible.

In conclusion, while the potential C—H···π interaction highlighted by the PLATON analysis is a factor to consider in the crystal packing of **K2**, the very small H—C···Cg (centroid) angle suggests that this interaction is weak and not as effective as hydrogen bonds in directing the crystal structure. Future studies may involve investigating the actual strength of this interaction using theoretical methods and making comparisons with similar structures, but the current geometry suggests that this interaction is not a dominant factor.

Investigation of void morphology and molecular packing properties of crystal structure

The structure and distribution of voids in crystal structures are of great importance in understanding the physical and chemical properties of the material. In this study, detailed analysis of voids and molecular packing arrangement in the internal structure of the crystal was performed using CrystalExplorer software. The analyses quantitatively reveal the volume, surface area and geometric complexity of voids in the crystal lattice, and also provide important information about the possible effects of these voids on molecular interactions.

Surface analyses performed with CrystalExplorer's Crystal Voids module show that there is a distinct and interconnected void network in the examined crystal structure. Visualization outputs reveal that the voids exhibit a continuous, complex three-dimensional structure formed by the regular interlocking of molecules and extending throughout the crystal. This void network presents an interlocking structure rather than isolated pockets and contributes significantly to the overall topology of the crystal.

As a result of the calculations, the void volume within the crystal unit cell was found to be 298.95 Å^3 and the void surface area was found to be 1063.72 Å^2 (Fig. 5). These values show that the crystal contains a significant amount of free volume despite its tightly packed appearance. In order to evaluate the shape properties of the voids, the calculated sphericity value was determined as 0.203 and the asphericity value as 0.340. A sphericity value considerably lower than 1 indicates that the voids have a rather irregular structure far from the ideal sphere geometry; a difference of the asphericity value from zero indicates that the voids have an unsymmetrical and complex morphology. These observations were also supported by visual analyses; the images obtained clearly revealed that the voids have a sponge-like, curved and porous structure.

This void network allows for various important inferences regarding the structural and functional properties of the crystal. When evaluated in terms of molecular packing, the free volume within the crystal emerges as a result of intermolecular interactions and shows that there are voids that allow molecular mobility even within the tightly packed structure. This may play a decisive role in terms of the overall stability of the crystal and diffusion processes at the molecular level.

In terms of the adsorption potential of the crystal, the interconnected structure of the voids and the large surface area make it possible to evaluate it as a potential adsorbent material. It is thought that small gas molecules, especially hydrogen (H_2), carbon dioxide (CO_2) and nitrogen (N_2), can diffuse into these voids. In order to experimentally verify this potential, it is recommended to perform complementary void analyses with software such as PLATON and also to perform gas adsorption isotherm experiments.

In terms of the mechanical and thermal properties of the crystal, the irregular and connected void network structure can have a direct effect on mechanical strength and thermal expansion behaviors. Such a structure can allow more effective distribution of internal stresses compared to densely packed crystal structures and can provide a more flexible response to temperature changes. In this context, it is also important to perform detailed thermomechanical analyses regarding the structural flexibility of the crystal.

As a result, this analysis performed with CrystalExplorer clearly revealed that the studied crystal structure has a high volume (298.95 Å^3) and large surface area (1063.72 Å^2), irregular (sphericity: 0.203) and complex (asphericity: 0.340) internal void network. The accessibility of this void structure, its effects on molecular adsorption capacity and mechanical properties may play an important role in determining the potential application areas of the material. In further studies, combining experimental gas adsorption analyses with modeling using different isovalue thresholds will illuminate the functional properties of these voids in more depth.

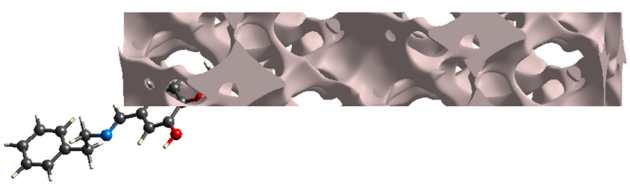

Fig. 5. Void network visualized within the crystal structure of the investigated molecule using CrystalExplorer software. The porous structure, rendered in grey, represents the intermolecular void spaces. The molecule is shown within the unit cell, illustrating its position and relationship with the void network. These voids originate from the molecular packing and exhibit a complex topology composed of interconnected yet narrow channels.

Computational studies

Hirshfeld surface analysis

Hirshfeld surface analysis has been conducted to verify the contributions of different intermolecular interactions in forming supramolecular structure. The intermolecular interactions in the refined crystal structure of the title compound have been examined using Hirshfeld surface analysis and fingerprint plots utilizing Crystal Explorer 17.5 [60]. Fingerprint plots with d_{norm} surface (where $d_{norm} = d_i + d_e$) for all intermolecular contacts, and the intermolecular energies of the molecular pairs in the crystal packing were calculated with molecular wavefunction at the B3LYP/6–311 G (d,p) level of theory, cluster of radius 3.8 Å around the molecule.

The Hirshfeld surface of the title compound have been mapped over d_{norm}, de, di, shape index, and curvedness (Fig. 6). The d_{norm} value is positive for longer contacts (blue region, d_{norm} > VdW radii), negative for shorter contacts (red regions, d_{norm} < VdW radii) compared to van der Waals separation (white regions, dnorm = VdW radii). The calculated molecular Hirshfeld surface area is 320.95 Å^2, which encloses the volume of 333.45 Å^3. Other calculated shape descriptors are globularity $G = 0.725$ and asphericity $\Omega = 0.481$.

The term a sphericity is a measure of structural anisotropy, and globularity is found as <1, indicating that the molecular surface is more structured [61–63]. Fig. 7 displays semitransparent d_{norm}-mapped the Hirshfeld surface for the title compound that form strong intermolecular contacts. The red regions in Fig. 7 are apparent around the nitrogen atom participating in the O—H···N and C—H···C contacts.

The 2D fingerprint plot provides a precise two-dimensional graphical representation of the intermolecular interactions in the crystal. The contributions from different contacts to the total Hirshfeld surface area are H···H (54.5 %), H···C/C···H (25.2 %), H···O/O···H (12.4 %), and H···N/N···H (3.8 %). The general contributions of the different contacts to the total Hirshfeld surface area are shown in Fig. 8.

Interaction energy calculations and energy frameworks

Using Crystal Explorer 17.5 built in feature, CE–B3LYP/6–31 G (d,p) energy model was applied to calculate the interaction energies in Fig. 7 [64–66]. Diagrammatical representation of energy frame works are represented in Fig. 9 (a,b,c). Energy frameworks calculation depicted that in the stabilization, dispersion energy contribution is dominated.

Molecular pairs involved in the calculation of the interaction energies of the title compound along a axis are shown in Fig. 7 (Table 2). The pictorial representation of Coulomb energy, dispersion energy, and the total interaction energy of the molecule viewed along a, b, and c axis is shown in green, red, and blue colors, respectively, and are displayed in Fig. 10. The total intermolecular interaction energy (E_{tot}) is the sum of four energy terms: electrostatic (E_{ele}), polarization (E_{pol}), dispersion (E_{disp}) and exchange-repulsion (E_{rep}) with scale factors of 1.057, 0.740, 0.871, and 0.618, respectively [65]. The different interaction energies viz., electrostatic, polarization, dispersion, and repulsion energies are −122, −32, −233, and 186.1 kJ/mol, respectively. The total energy is

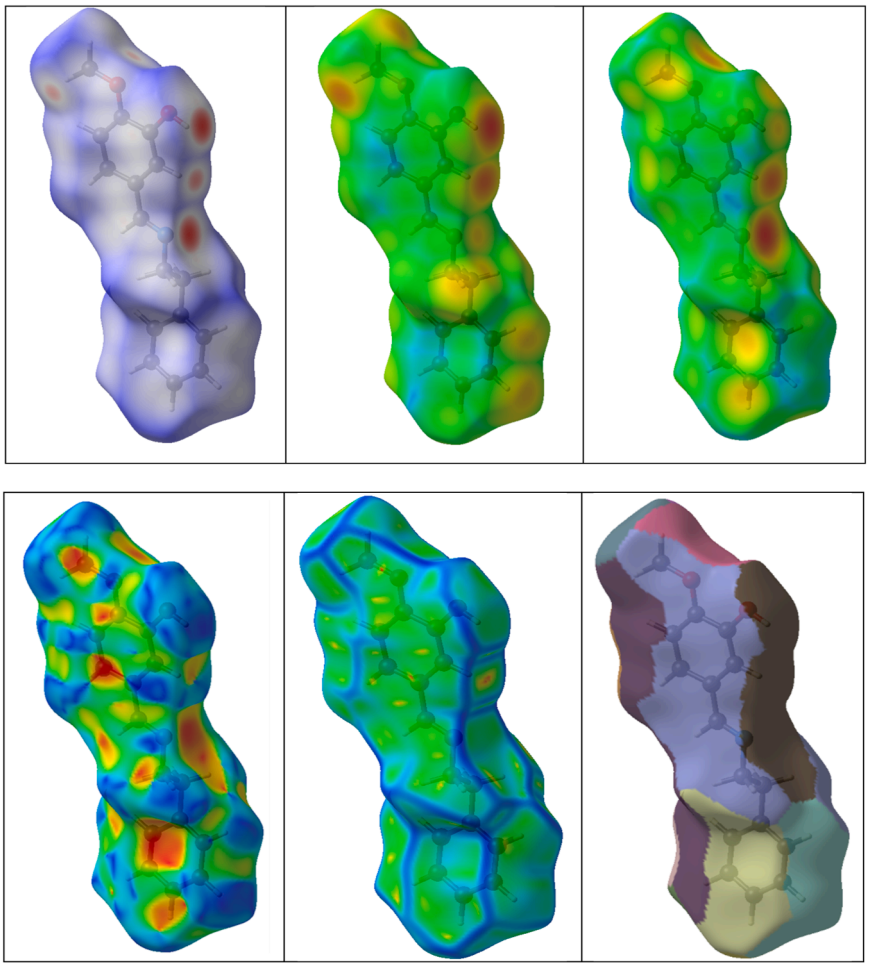

Fig. 6. Hirshfeld surface mapped with d_{norm} (a), d_e (b), d_i (c), shape index (d), curvedness (e) and fragment patch (f) for the title compound.

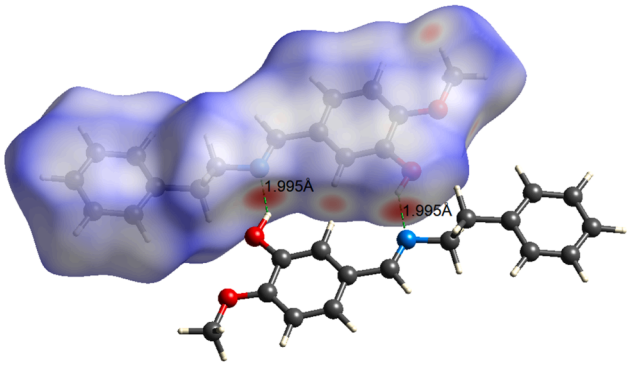

Fig. 7. d_{norm} map showing regions intermolecular contacts over the title compound.

−240.4 kJ/mol. The cylinders in the energy framework depict the relative strengths of the molecular packing and the associated energies between the molecular pairs in different directions, while the absence of cylinders along a particular direction is due to weak interactions below a threshold energy (5 kJ/mol) and they are omitted.

The dispersion of energy framework is dominant over the electrostatic energy framework shown in Fig. 10 and Table 3.

DFT studies

Geometry optimization of synthesized compound was done by using B3LYP/6–31 G (d,p) basis set. All theoretical calculations were performed using Density Functional Theory (DFT) with the B3LYP functional. The 6–31G(d,p) basis set was employed for all C, N, O, and H atoms. This specific basis set was chosen due to its split-valence nature, which provides a flexible description of valence electrons, crucial for accurate bonding and molecular geometry. Furthermore, the inclusion of polarization functions (d for heavy atoms and p for hydrogen atoms) is essential for a precise description of bond angles, lone pairs, and charge distributions, particularly important in a polar molecule like **K2**. This choice represents a well-established balance between computational efficiency and the required accuracy for the studied molecular properties, including geometry, electronic structure (HOMO-LUMO), dipole moment, and polarizability. Optimized structure of synthesized compound **K2** is shown in Fig. 11.

Frontier molecular orbital analysis

The chemical, optical, and electronic characteristics of molecules are largely determined by their frontier orbitals.

FMO is an indicator of electron occupancy, LUMO denotes the lowest electron occupancy while the HOMO depicts the highest occupied molecular orbital. FMO (Frontier Molecular Orbital) calculations have a major role in reactivity and stability assessment. HOMO and LUMO representation of **K2** are given in Fig. 12. Using B3LYP/6–31 G (d,p), frontier molecular orbitals were calculated. LUMO and HOMO energies were found to be −0.11707 and −0.2820 respectively. Highest Occupied Molecular Orbital (HOMO) analysis revealed that maximum delocalization was observed at the nitrogen atom. LUMO analysis depicts that

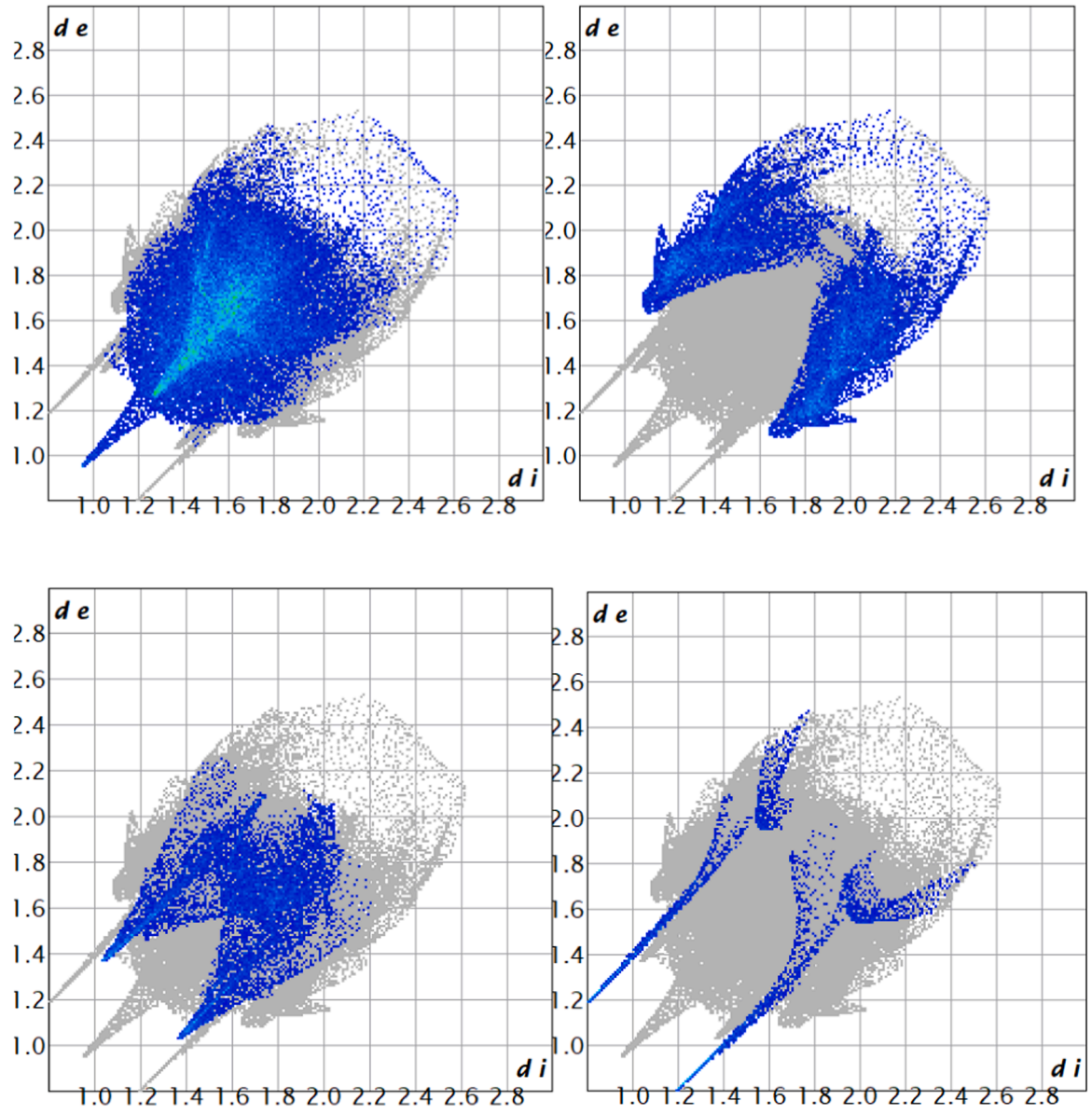

Fig. 8. 2-Dimensional fingerprint plot of the main intermolecular interactions in the crystal structure of the title compound.

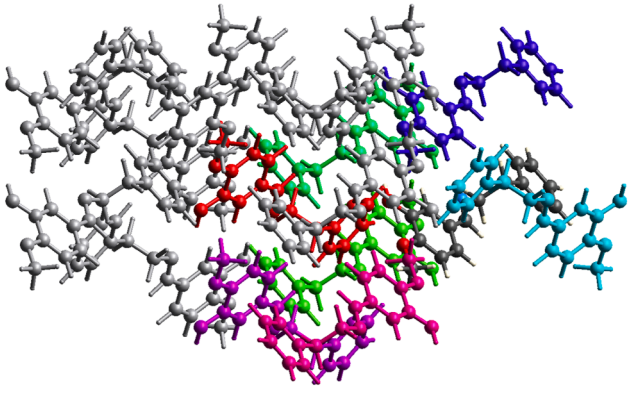

Fig. 9. Molecular pairs involved in the calculation of interaction energies of the title compound along *a axis*.

the hexane ring exhibits the greatest degree of delocalization. However, electron density is usually concentrated at the center where heteroatoms are present. Values of various physical and Global Chemical Reactivity Descriptors properties are given in Tables 4 and 5.

The electronic and reactivity parameters of **K2** compound obtained by DFT calculations are presented in Table 4 and Table 5 of this study. These values provide important information about the potential biological and chemical applications of the molecule. Our findings are consistent with the results obtained by DFT studies of similar organic molecules and reported in the literature.

First of all, it is noteworthy that the HOMO-LUMO energy gap (ΔEgap) of **K2** is quite small, 0.164 eV [Table 4]. Similarly, in a study on purine analogues, it was stated that DFT analyses provide valuable information about the electronic properties related to the cytotoxic and antioxidant activities of molecules [67]. Smaller energy gaps are generally associated with lower excitation energies and higher reactivity, since the transition of electrons from HOMO to LUMO requires less energy. This is a critical factor for both the experimentally observed antioxidant and antimicrobial activities of **K2**, since such activities are usually directly related to electron transfer processes [68,69]. In

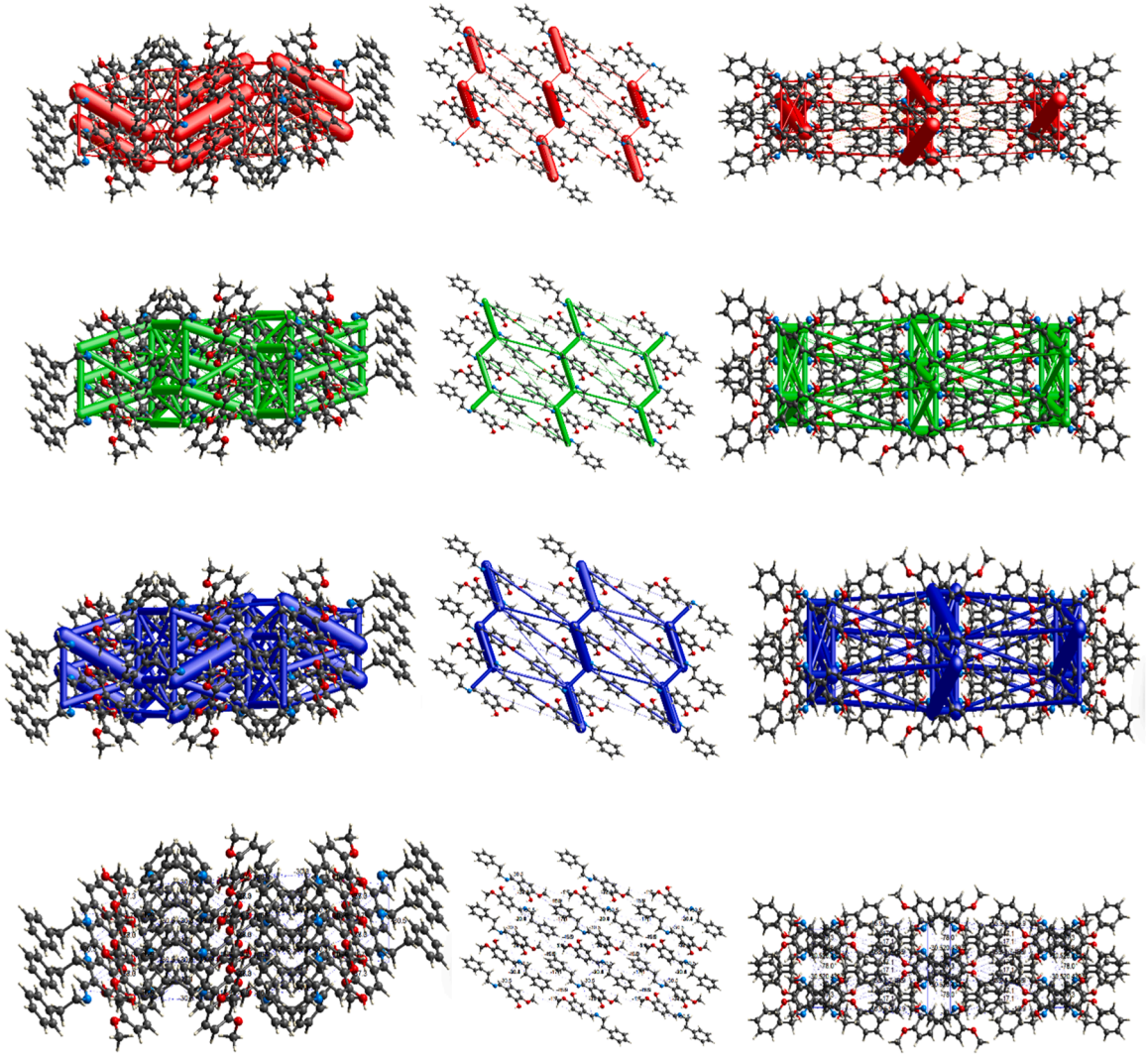

Fig. 10. Representation of the Coulomb interaction energy, dispersion energy, and total energy in red, green, and blue colors along the *a, b*, and *c axes*, respectively.

Table 3
Different interaction energies of molecular pairs in kJ/mol.

	N	Symop	R	Electron Density	E_ele	E_pol	E_dis	E_rep	E_tot
	1	x+1/2, -y+1/2, z+1/2	15.68	B3LYP/6-31G(d,p)	-6.3	-1.5	-10.5	0.0	-16.9
	0	-x, y, -z+1/2	6.96	B3LYP/6-31G(d,p)	-7.1	-1.3	-24.4	15.0	-20.4
	0	-x+1/2, -y+1/2, -z	16.06	B3LYP/6-31G(d,p)	-1.9	-0.1	-4.4	0.0	-5.9
	1	-x, -y, -z	6.10	B3LYP/6-31G(d,p)	-5.2	-3.8	-58.2	35.1	-37.3
	1	-x, -y, -z	6.65	B3LYP/6-31G(d,p)	-86.0	-20.5	-31.0	89.2	-78.0
	1	-x, y, -z+1/2	4.23	B3LYP/6-31G(d,p)	-5.3	-1.7	-46.6	26.9	-30.8
	0	-x+1/2, y+1/2, -z+1/2	12.16	B3LYP/6-31G(d,p)	-0.6	-0.6	-18.5	0.0	-17.1
	1	x, y, z	5.52	B3LYP/6-31G(d,p)	-11.3	-2.1	-33.7	19.9	-30.5
	1	x+1/2, -y+1/2, z+1/2	16.41	B3LYP/6-31G(d,p)	1.2	-0.2	-3.4	0.0	-1.8
	1	-x+1/2, -y+1/2, -z	17.12	B3LYP/6-31G(d,p)	0.5	-0.2	-2.3	0.0	-1.7

* The color and compound relationship are given in Fig. 9.

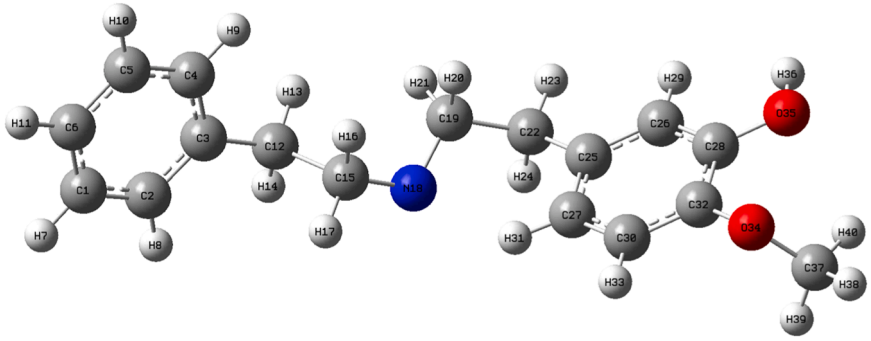

Fig. 11. Optimized structure of **K2**.

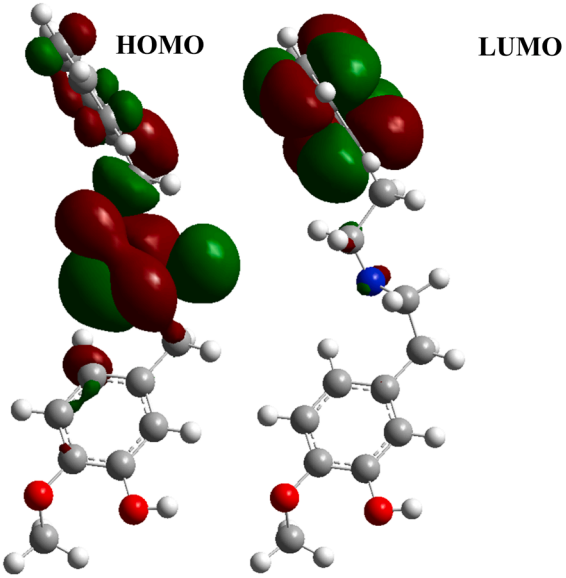

Fig. 12. HOMO and LUMO representation of **K2**.

Table 4
Physical Parameters of **K2.**

Optimization Energy (Hartree)	Polarizability a.u.	Dipole Moment	ΔEgap (eV)	Softness (S)	Hardness (η)
−865.028985	399.9394	4.654888	0.164	0.340	0.223

Table 5
Global Chemical Reactivity Descriptors.

E.A	I.E	(ω)	(ω-)	(ω+)	(Δω±) (X)
0.11707	0.2820	0.259	0.241	0.041	0.282 −0.340

E.A: Electron Affinity, I.E: Ionization Energy, (ω): Electrophilicity Index, (ω-): Electron donating Power, (ω+): Electron Accepting Power, (Δω±): Net Electrophilicity, (X): Electronegativity.

particular, DFT is also used to understand such relationships in studies investigating the biological activities of isatin derivatives [70].

The high polarizability value of **K2** (399.9394 a.u.) and significant dipole moment (4.654888 D) [Table 5] indicate that the electronic structure of the molecule is sensitive to external effects and has a polar structure. These features are frequently emphasized by DFT analyses, especially in studies focusing on the design of new chemical sensors (e.g. Fe3O4@SiO2-Pr-NH-IC, SBA-Pr-Ald-MA and other metal ion sensors) [71–73]. The high polarizability supports the 'soft' character of the molecule (hardness η = 0.223, softness S = 0.340) [70] and thus indicates higher reactivity.

In addition, the electron donor power (ω- = 0.241) value of **K2** is higher than the electron acceptor power (ω+ = 0.041) value [Table 5], indicating that the molecule has a stronger tendency to act as an electron donor. This finding is directly consistent with the antioxidant activity of **K2**, which explains its ability to neutralize free radicals through electron donation. Similarly, the study on purine analogues has also indicated that DFT insights contribute to the understanding of antioxidant activities [70].

In summary, the electronic and reactivity parameters of **K2**, such as low band gap, high polarizability, significant dipole moment and electron donation tendency determined by DFT calculations, are strongly consistent with the results obtained from similar studies in the literature. These comparisons emphasize that the electronic structure of **K2** supports its biological activities and is potentially a valuable compound for various applications.

Antioxidant results

Free radicals are extremely unstable and highly reactive due to their unpaired electrons. These unstable intermediates easily exchange electrons with other stable molecules. Overproduction of free radicals, which are continuously produced during normal physiological activities, can lead to cell damage, which in turn causes serious diseases such as cancer, hypertension, aging, atherosclerosis, and Alzheimer's disease [74]. Antioxidants play a crucial role in counteracting the harmful effects of ROS and free radicals, even at low concentrations, and help reduce oxidative stress in the human body and food systems by significantly reducing the accumulation of free radicals, thereby alleviating potential damage [75].

Schiff bases contain hydroxy groups in their chemical structures and can block the harmful effects of free radicals of antioxidants [76]. Previous in vitro experiments have shown that antioxidant activity determinations may differ [74,77]. The DPPH• experiment is carried out in 50 % ethanol/water solution, while the $ABTS^{\bullet+}$ experiment is carried out in aqueous medium; these differences may lead to differences in radical scavenging activities. The solubility of the compounds in both media is important; some bioactive compounds may not show activity because they are insoluble. While the $ABTS^{\bullet+}$ experiment works with cation radicals and the DPPH• experiment works with free radicals, the FRAP experiment is based on the reducing power of the compound to iron ions [77]. In this study, the antioxidant capacities of the Schiff base compound were evaluated using two methods and the results are given in Table 6.

When evaluated by the DPPH• method, the compounds must have strong hydrogen donor groups to exhibit good antioxidant properties [78]. The DPPH• activity of the synthesized compounds is given in Table 6. This compound showed lower antioxidant activity compared to Trolox (Table 6). The antioxidant potential of the synthesized Schiff bases was confirmed by their $ABTS^{\bullet+}$ radical scavenging activities.

Table 6
The reducing ability of Schiff base (**K2**) by DPPH•, $ABTS^{\bullet+}$, Fe^{3+} Reducing, CUPRAC reducing methods.

Compounds	DPPH• Scavenging		$ABTS^{\bullet+}$ Scavenging	
	IC_{50}	R^2	IC_{50}	R^2
K2	188.98	0.9924	10.63	0.9839
Trolox	7.74	0.9950	6.94	0.9912
	Fe^{3+} Reducing		**Cu^{2+} Reducing**	
	λ_{700} *	R^2	λ_{450} *	R^2
K2	0.186 ± 0.003	0.9982	2.11 ± 0.081	0.9959
Trolox	1.095 ± 0.053	0.9807	0.929 ± 0.051	0.9807

IC_{50} (μg/mL) values for DPPH• and $ABTS^{\bullet+}$ scavenging abilities.
* At a concentration of 50 μg/mL, the values are expressed as absorbance.

$ABTS^{\bullet+}$ radical test is a traditional and effective model to evaluate the activities of hydrogen donating and chain breaking antioxidants [31]. The IC_{50} value for $ABTS^{\bullet+}$ activity of the synthesized compound was 10.63 μg/mL. This compound showed lower $ABTS^{\bullet+}$ activity than trolox (Table 6).

Another important parameter for the evaluation of antioxidant activity is the reducing power of the compounds. It is measured as the reduction of Fe $^{3+}$ (ferricyanide) complex to Fe^{2+} form. As given in Table 5, compound **K2** showed high ferric reducing power activity of 0.186 ± 0.003.

In the presence of antioxidants, the blue-green bis(neocuproine)-Cu (II) chelate is reduced to the yellow-orange bis(neocuproine)-Cu(I) charge transfer complex via outer sphere single electron transfer. This complex absorbs at 450 nm wavelength and this absorbance value is used to determine the antioxidant activity level [79]. When Cu^{2+} reduction capacity was evaluated, compound **K2** (2,11 ± 0081) exhibited a higher reduction capacity compared to Trolox (0929 ± 0, 0924).

Antimicrobial activity

Bacterial infections are a serious concern for global health. Antibiotics are a widely used strategy in the treatment of these infections today; however, the misuse of antibiotics poses a major threat to human health by leading to the emergence of drug-resistant bacteria [75]. Therefore, the development of new and effective antibacterial agents is important as an additional strategy to the rational use of existing antibiotics. Schiff bases are compounds that can complex with metal ions and exhibit antimicrobial activity. These complexes generally act on the cell walls and membranes of microorganisms, inhibiting their growth and reproduction. These properties make Schiff bases valuable as potential antimicrobial agents [80]. In our research, the potential antibacterial activities of the synthesized Schiff base compound were evaluated against bacteria such as *Staphylococcus aureus* (ATCC 25213), *Bacillus cereus* (709 Rome), *Enterococcus faecalis* (ATCC 29212), *Listeria monocytogenes* (ATCC 43251), *Acinetobacter baumannii* (ATCC 02026), *Klebsiella pneumoniae* (ATCC 10031), *E. coli* (ATCC 25922) and *Pseudomonas aeruginosa* (ATCC 43288) using the agar well diffusion method. Gentamicin (GN) and Ciprofloxacin (CIP) were tested under the same conditions. Schiff base (**K2**) was found to have different degrees of inhibitory effect on gram positive and gram negative bacteria and the inhibition zone diameters varied between 13–21 mm (Table 7).

Compound **K2** showed inhibition zones of 14, 14, 13, 13, 13, 21, 14 and 14 mm in diameter against *S. aureus, B. cereus, E. faecalis*, L. *monocytogenes, A. baumannii, K. pneumoniae* and *E. coli*, respectively. No antibacterial effect was detected against *P. aeruginosa*. The tested compound showed a 22 mm inhibition zone against *A. baumannii*, which was higher than the inhibition zones of GN (21 mm) and CIP (20 mm) (Table 7). These results highlight the promising antimicrobial efficacy of compound **K2**, a β-phenylethylamine derivative Schiff base, particularly against multidrug-resistant Gram-negative strains. The presence of imine (–*C* = *N*–) and hydroxyl groups in its structure may enhance its ability to disrupt bacterial cell wall integrity or interfere with essential microbial enzymes [81]. Its increased activity against *A. baumannii* is especially noteworthy, considering the clinical relevance of this pathogen [82].

This compound showed inhibitory activity against *A. baumannii* (21 mm) close to the standard antibiotics tested. This pathogen is a gram-negative bacterium commonly found in hospital environments, known for its high-level resistance to many antibiotics. Its resistance to carbapenem antibiotics in particular limits treatment options and leads to difficult-to-treat infections [83].

The results suggest that compound **K2** is a potentially promising therapeutic antibacterial agent. Inhibitory activity is enhanced by the hydrogen bonds of the hydroxyl and azomethine groups in compound **K2** with the active centers of cellular structures [84]. The hydrophobicity of these compounds is the main factor that facilitates passage through the cell membrane, while their polarity is critical for efficacy. Studies have shown that compounds containing hydrogen bonds are effective against microorganisms. In addition, it is known that antibiotic substances can easily react with liposaccharides loaded with active groups such as –OH and –NH, thus facilitating drug absorption [84,85].

Molecular docking studies

Molecular docking study provides a clearer picture of the research focus by examining the interactions with specific target receptors and sheds light on the efficacy of the compounds [86].

In this study, four proteins, 1NHJ (N-terminal 40KD MutL/A100P mutant protein complex with ADPnP and one sodium), 3QX3 (Human topoisomerase-II beta in complex with DNA and etoposide, 2XO8 (cytochrome c peroxidase: ascorbate bound to the engineered ascorbate binding site) and 1HD2 (Human peroxiredoxin 5) (antioxidant receptor) (HP5) were used to perform docking analyses with the synthesized compound (**K2**). The docking results of compound **K2** and the interactions of this compound with the residues in the active site of the enzyme were determined (Fig. 10–13).

K2 exhibited good binding interactions with 1NHJ residues, with a binding energy of −6.22 kcal/mol (Fig. 13). It showed π-sigma interactions were with LEU220 (3.72 A^o). π-Alkyl interactions were with PHE213 (5.35 A^o), ILE250 (4.55 A^o), ALA246 (4.03 and 4.77 A^o), VAL212 (5.35 A^o) residues, π-π T-Shaped interactions was with PHE213 (5.84 A^o) residues of 1NHJ. Van der Waals interactions were observed between PRO243, ALA303, PHE304, GLY209, ASN210, MET207, THR37, ASN247, ILE156 and ALA213.

Table 7
Inhibition zones in mm diameter for the synthesized compounds.

	Diameter of inhibition zone (mm)							
	S. aureus (ATCC 25213)	*B. cereus (709 Roma)*	*E. faecalis* (ATCC 29212)	*L. monocytogenes* (ATCC 43251)	*A.baumannii (ATCC 02026)*	*K. pneumoniae* (ATCC 10031)	*E. coli (ATCC 25922)*	*P. aeruginosa (ATCC 43288)*
K2	14	14	13	13	21	14	14	n.d.
GN	18	21	n.d	n.d.	21	18	19	17
CIP	22	19	20	n.d.	20	21	22	27

GN: Gentamisin, CIP: Ciprofloxacin, n.d: Not detected.

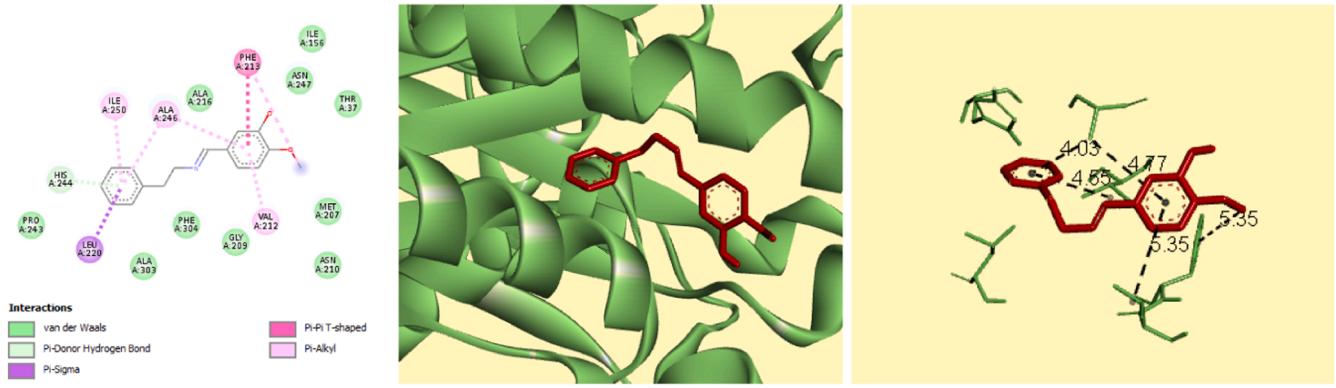

Fig. 13. 2D and 3D showing bond interactions of **K2** with active site residues of N-terminal 40KD MutL/A100P mutant protein complex with ADPnP and one sodium (PDB: 1NHJ).

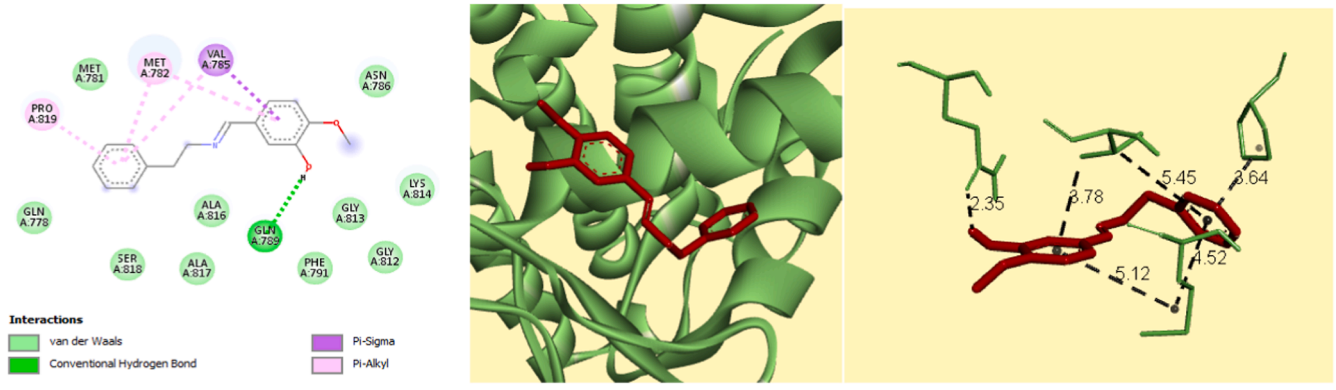

Fig. 14. 2D and 3D showing bond interactions of **K2** with active site residues of Human topoisomerase-II beta in complex with DNA and etoposide (PDB: 3QX3).

K2 exhibited good binding interactions with 3QX3 residues, with a binding energy of −6.03 kcal/mol. **K2,** as seen from the Fig. 14, conventional hydrogen bond was observed between GLN789 residue with the 2.35 A^{o} bond length. The π-alkyl interactions were observed between MET782, PRO819, VAL785 residues and the center of phenyl ring with 5.12 and 4.52, 3.64 and 5.45 A bond lengths, respectively. Additionally, π-sigma interactions were observed between VAL785 residue with 3.78 A^{o} bond length. Van der Waals interactions were observed between GLN778, SER818, ALA817, ALA816, PHE791, GLY813, GLY812, LYS814, ASN786 and MET781.

K2 exhibited good binding interactions with 2XO8 residues, with a binding energy of −6.47 kcal/mol. **K2,** as seen from the Fig. 15, conventional hydrogen bond was observed between GLU467 residue with the 1.90 A^{o} bond length. C—H bond was observed between GLU467 residue with the 2.95 A^{o} bond length. π-Donor interaction was observed between LEU263 residue with 2.64 A^{o} bond length. The alkyl interactions were observed between LYS587 residue and the center of phenyl ring with 3.54 bond length. π-Sigma interaction was observed between LYS265 residue with 3.66 and 3.76 A^{o} bond length. Additionally, Van der Waals interactions were observed between LEU431, TYR261, GLN637, LEU262, VAL630,LYS423, SEER266,GLU264 and TYR634.

K2 exhibited good binding interactions with 1HD2 residues, with a binding energy of −7.45 kcal/mol. **K2,** as seen from the Fig. 16, conventional hydrogen bond was observed between VAL70 residue with the 1.84 A^{o} bond length. C-H bond was observed between LYS93 residue

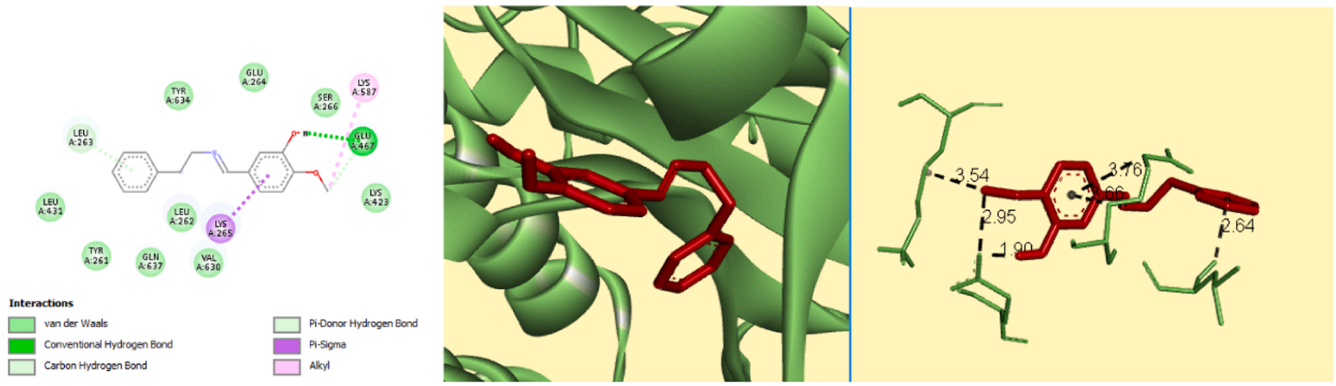

Fig. 15. 2D and 3D showing bond interactions of **K2** with active site residues of cytochrome c peroxidase: ascorbate bound to the engineered ascorbate binding site (PDB: 2XO8).

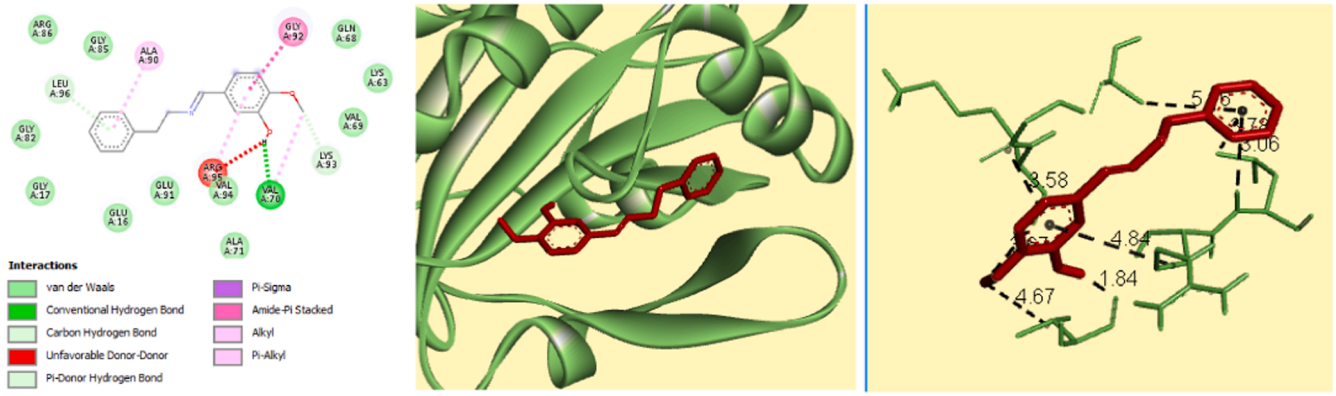

Fig. 16. 2D and 3D showing bond interactions of **K2** with active site residues of Human peroxiredoxin 5 (antioxidant receptor) (PDB: 1HD2).

with the 3.67 A^o bond length. π-Donor interaction was observed between LEU96 residue with 3.06 A^o bond length, Also amide-pi stacked was observed GLY92 residue with 3.58 A^o bond length. The alkyl interactions were observed between VAL70 residue and the center of phenyl ring with 4.67 bond length. Additionally, π-Sigma interaction was observed between LEU96 residue with 3.78 A^o bond length, Pİ-alkyl interaction was observed between ALA90, ARG95 residue with 5.16 and 4.84 A^o bond lengths, respectively. Van der Waals interactions were observed between ARG86, GLY85, GLN68, LYS63, VAL69, ALA71, VAL94, GLU91, GLU16, GLY17 and GLY82.

Conclusion

In this study, the newly synthesized Schiff base (E)-5-(((4-(dimethylamino)phenyl)imino)methyl)-2-methoxy phenol (**K2**) was investigated by various characterization techniques and its biological activities were evaluated in detail. Advanced techniques such as ^{1}H and ^{13}C NMR, HRMS and X-ray diffraction were used for structural characterization. Single crystal X-ray diffraction analysis confirmed that **K2** crystallizes in the monoclinic C2/c space group with cell parameters $a = 27.794$ (2) Å, $b = 5.5186$ (4) Å, $c = 17.8651$ (15) Å, and β =96.341 (3) °. In particular, the constitutive hydrogen bonds between the hydroxyl group and nitrogen/oxygen atoms were identified as critical for the crystal packing. Hirshfeld surface analysis highlighted H (54.5 %) and H C/C H (25.2 %) interactions as dominant. DFT calculations revealed a low energy band gap of 0.164 eV and a dipole moment of 4.65 Debye, indicating high reactivity and polarizability for **K2**.

The biological profile of compound **K2** was comprehensively assessed, confirming its antimicrobial efficacy against both Gram-positive and Gram-negative bacteria and its strong antioxidant potential through multiple in vitro assays. These results support its potential role in addressing both bacterial infections and oxidative stress-related conditions.

Furthermore, molecular docking simulations were performed to investigate the interaction of **K2** with biologically relevant proteins. The compound showed favorable binding affinity with all four target proteins examined: 1NHJ, 3QX3, 2XO8, and 1HD2. **K2** showed the strongest binding interaction with Human Peroxiredoxin 5 (1HD2), an antioxidant receptor, with a binding energy of −7.45 kcal/mol. This suggests that **K2** has a high affinity for antioxidant enzymes. Additionally, a binding energy of −6.47 kcal/mol was observed for the interaction between **K2** and Cytochrome c peroxidase (2XO8), indicating a remarkable interaction. **K2** also showed significant binding affinities with Human Topoisomerase-II beta (3QX3) and MutL/A100P mutant protein complex (1NHJ) with binding energies of −6.03 kcal/mol and −6.22 kcal/mol, respectively. In general, **K2** showed stable and strong binding interactions with all the proteins examined. These findings suggest that **K2** may have potential biological activities and may be a promising candidate, especially in antioxidant-related mechanisms.

Among these, the strongest interaction was observed with Human Peroxiredoxin 5 (1HD2), an antioxidant enzyme with a binding energy of −7.45 kcal/mol. This was followed by interactions with Cytochrome c peroxidase (2XO8) at −6.47 kcal/mol, MutL/A100P mutant protein complex (1NHJ) at −6.22 kcal/mol, and Human Topoisomerase II beta (3QX3) at −6.03 kcal/mol. These results suggest a consistent and positive interaction pattern, especially with proteins involved in oxidative stress responses.

In conclusion, the findings obtained in this study show that compound **K2** has antimicrobial and antioxidant properties and holds significant potential in the field of health in these aspects. The structural and electronic properties of **K2** make it a promising candidate for pharmaceutical and biomedical applications. Notably, compound **K2** exhibited high antimicrobial activity against *Acinetobacter baumannii*, a critical multidrug-resistant pathogen, highlighting its potential as a valuable candidate in the fight against antibiotic-resistant infections. These findings provide a promising basis for the potential use of **K2** in the design of new therapeutic agents targeting oxidative stress-related diseases and bacterial infections, especially in this era of increasing antibiotic resistance.

Data availability

Crystallographic data

Crystallographic data for the structure of K2 have been deposited with the Cambridge Crystallographic Data Centre (CCDC) under deposition number **2441556**. These data can be obtained free of charge from the CCDC via www.ccdc.cam.ac.uk/data_request/cif.

The data that support the findings of this study are available from the corresponding author upon reasonable request.

CRediT authorship contribution statement

Kübra Öztürk: Writing – original draft, Resources, Investigation, Conceptualization. **Ebrar Nur Özkan:** Writing – review & editing, Software, Resources, Investigation, Formal analysis. **Çiğdem Er Çalışkan:** Writing – review & editing, Investigation, Conceptualization. **Sertan Aytaç:** Writing – review & editing, Methodology, Conceptualization. **Özlem Gündoğdu Aytaç:** Writing – original draft, Supervision, Resources, Investigation, Conceptualization.

Declaration of competing interest

The authors declare that they have no known competing financial interests or personal relationships that could have appeared to influence the work reported in this paper.

Acknowledgements

The authors would like to thank Ataturk University and Kırşehir Ahi Evran University for the facilities and technical support. This study was supported by Kırşehir Ahi Evran University Scientific Research Projects (BAP) project numbered MMF.A3.24.003.

Supplementary materials

Supplementary material associated with this article can be found, in the online version, at doi:10.1016/j.molstruc.2025.143011.

References

[1] K. Poturcu, E.Ç. Demiralay, Determination of ionisation/protonation, lipophilicity and solubility constants of some heterocyclic compounds, J. Süleyman Demirel Univ. Grad. Sch. Sci. Technol. 23 (2) (2019) 651–657.
[2] P. Moyano, J. Del Pino, Monoamine neurotransmission and toxicity, (2024).
[3] S.R. Haadsma-Svensson, K.A. Svensson, PNU-99194A: a preferential dopamine D3 receptor antagonist, CNS. Drug Rev. 4 (1) (1998) 42–53.
[4] K. Aksu, Synthesis of sulfamide derivatives of dopamine-like compounds, 2014.
[5] P. Riederer, G. Laux, MAO-inhibitors in Parkinson's Disease, Exp. Neurobiol. 20 (1) (2011) 1.
[6] N. Kaur, B. Kumari, Phenylethylamıne: health benefits-A revıew, World J Pharm Pharma Sci 5 (4) (2016) 743–750.
[7] I.H. Hatim, W.A. Al-Masoudi, R.F. Ghadhban, Synthesis, characterization and acute toxicity of new Schiff base derived from phenylethyl amine and 2-hydroxy naphthaldehyde, Eur. J. Chem. 10 (1) (2019) 26–29.
[8] S. Aytaç, Resynthesis of schiff base compounds with an environmentally friendly method, J. Inst. Sci. Technol. 11 (4) (2021) 2979–2991.
[9] E. Vitaku, D.T. Smith, J.T. Njardarson, Analysis of the structural diversity, substitution patterns, and frequency of nitrogen heterocycles among US FDA approved pharmaceuticals: miniperspective, J. Med. Chem 57 (24) (2014) 10257–10274.
[10] H. Ömerustaoğlu, Synthesis and Characterization of 5-Pyrazolone-Urea Derived Schiff Bases, Ordu University, Institute of Science, Yüksek Lisans Tezi (Basılmış, 2017.
[11] S.G. Nayak, B. Poojary, Synthesis of novel Schiff bases containing arylpyrimidines as promising antibacterial agents, Heliyon. 5 (8) (2019).
[12] H. Kargar, M. Ashfaq, M. Fallah-Mehrjardi, R. Behjatmanesh-Ardakani, K. S. Munawar, M.N. Tahir, Theoretical studies, Hirshfeld surface analysis, and crystal structure determination of a newly synthesized benzothiazole copper (II) complex, J. Mol. Struct. 1261 (2022) 132905.
[13] A.M.N. Khaleel, M.I. Jaafar, Synthesis and characterization of boron and 2-aminophenol Schiff base ligands with their Cu (II) and Pt (IV) complexes and evaluation as antimicrobial agents, Orient. J. Chem. 33 (5) (2017) 2394–2404.
[14] S. Aytaç, Synthesis of pyridine-based imine compounds and molecular docking studies against dopamine D2 receptors, Hittite J. Sci. Eng. 10 (2) (2023) 161–165.
[15] S. Aytaç, Ö.G. Aytaç, Eco-friendly synthesis of new thiophene-based Schiff bases containing piperidine rings, Org. Commun. 17 (2) (2024) 132.
[16] N. Birbiçer, Synthesis of metal complexes of water soluble dyes and investigation of dye properties, (1998).
[17] V.n. Macho, M. Králik, J. Hudec, J. Cingelova, One stage preparation of Schiff's bases from nitroarenes, aldehydes and carbon monoxide at presence of water, J. Mol. Catal. A: Chem. 209 (1–2) (2004) 69–73.
[18] M. Bal, Synthesis of new azo-schiff base type ligand and metal complexes, investigation of their spectroscopic and genotoxic properties, Kahramanmaraş Sütçü İmam University (2010).
[19] M. Ayaz, Ö. Gündoğdu, S. Aytaç, B. Erdem, H. Çiftçi, Y. Erdogdu, Microwave-assisted synthesis, characterizations, antimicrobial activities, and DFT studies on some pyridine derived Schiff bases, J. Mol. Struct. 1269 (2022) 133791.
[20] M. Salehia, M. Maciej Kubickib, M.G. Jafaria, F. Soleimania, Synthesis, crystal structure, spectroscopic, molecular docking and DFT studies of two Schiff base ligands derived from DL-1-phenylethylamine, J. Appl. Chem. 13 (49) (2019).
[21] A. Hssaın, DFT modelling studies of spectroscopic properties and medium effects on molecular reactivity of secnidazole in different solvents, J. Phys. Chem. Funct. Mater. 5 (1) (2022) 69–83.
[22] N. Damar, G.K. Balcı, Investigation of structural, electronic and magnetic properties of DyCuPb and YCuPb compounds using density functional theory (DFT), Dicle Univ. J. Sci. Inst. 8 (2) (2019) 8–14.
[23] P. Prabhakaran, S. Kanagasabai, G. Seshan, K. Gugan, S. Usharani, P. Rajakumar, Crystal structure and hirshfeld surface analysis of 1, 2, 3, triazole bridged pyrrolizidine grafted macrocycle, Chem. Data Collect. 28 (2020) 100427.
[24] S. Aytac, O. Gundogdu, Z. Bingol, İ. Gulcin, Synthesis of Schiff bases containing phenol rings and investigation of their antioxidant capacity, anticholinesterase, butyrylcholinesterase, and carbonic anhydrase inhibition properties, Pharmaceutics. 15 (3) (2023) 779.
[25] T. Gruene, H.W. Hahn, A.V. Luebben, F. Meilleur, G.M. Sheldrick, Refinement of macromolecular structures against neutron data with SHELXL2013, Appl. Crystallogr. 47 (1) (2014) 462–466.
[26] L. Bourhis, O. Dolomanov, R. Gildea, J. Howard, H. Puschmann, C31 (H31), C34 (H34), C19 (H19), C22 (H22) 2. b aromatic/amide H refined with riding coordinates: C15 (H15), C18 (H18), C29 (H29), C2 (H2), C12 (H12), C26 (H26), C16 (H16), C28 (H28), C3 (H3), C27 (H27), C8 (H8), C17 (H17), C11 (H11), C9 (H9), C10 (H10), C4 (H4), C6 (H6), C5 (H5), J. Appl. Cryst 42 (2009) 339–341.
[27] L. Bourhis, O. Dolomanov, R. Gildea, J. Howard, H. Puschmann, C168–C166= C167–C166= C164–C163= C165–C163= C162–C160= C161–C160= C159–C157= C158–C157 1.54 with sigma of 0.002 O41–C157= O42–C160= O44–C166= O43–C163 1.23 with sigma of 0.002, J. Appl. Cryst 71 (2015) 59–75.
[28] G.M. Sheldrick, Crystal structure refinement with SHELXL, Cryst. Struct. Commun. 71 (1) (2015) 3–8.
[29] R. Apak, A. Calokerinos, S. Gorinstein, M.A. Segundo, D.B. Hibbert, İ. Gülçin, S. Demirci Çekiç, K. Güçlü, M. Özyürek, S.E. Çelik, Methods to evaluate the scavenging activity of antioxidants toward reactive oxygen and nitrogen species (IUPAC Technical Report), Pure Appl. Chem. 94 (1) (2022) 87–144.
[30] M.S. Blois, Antioxidant determinations by the use of a stable free radical, Nature 181 (4617) (1958) 1199–1200.
[31] R. Re, N. Pellegrini, A. Proteggente, A. Pannala, M. Yang, C. Rice-Evans, Antioxidant activity applying an improved ABTS radical cation decolorization assay, Free radic. biol. med. 26 (9–10) (1999) 1231–1237.
[32] Á. Nagy, Density functional. Theory and application to atoms and molecules, Phys. Rep. 298 (1) (1998) 1–79.
[33] M. Frisch, G.W.;. Schlegel, et al., Gaussian 09, Revision D. 01, Gaussian, Inc., Wallingford CT, 2009.
[34] I. Mahmudov, Y. Demir, Y. Sert, Y. Abdullayev, A. Sujayev, S.H. Alwasel, I. Gulcin, Synthesis and inhibition profiles of N-benzyl-and N-allyl aniline derivatives against carbonic anhydrase and acetylcholinesterase–A molecular docking study, Arab. J. Chem. 15 (3) (2022) 103645.
[35] X. Hu, M. Machius, W. Yang, Monovalent cation dependence and preference of GHKL ATPases and kinases, FEBS Lett. 544 (1–3) (2003) 268–273.
[36] M. Anza, M. Endale, L. Cardona, D. Cortes, R. Eswaramoorthy, J. Zueco, H. Rico, M. Trelis, B. Abarca, Antimicrobial activity, in silico molecular docking, ADMET and DFT analysis of secondary metabolites from roots of three Ethiopian medicinal plants, Adv. Appl. Bioinform. Chem. (2021) 117–132.
[37] W.S. Shehab, M. Abdelaziz, N.K.R. Elhoseni, M.G. Assy, M.H. Abdellattif, E. O. Hamed, Design, synthesis, molecular docking, and evaluation antioxidant and antimicrobial activities for novel 3-phenylimidazolidin-4-one and 2-aminothiazol-4-one derivatives, Molecules. 27 (3) (2022) 767.
[38] E. Korkusuz, Y. Sert, E. Selvi, H. Aydın, İ. Koca, İ. YILDIRIM, Molecular docking and antioxidant activity studies of imidodithiocarbonate derivatives containing pyrimidine, Org. Commun. 16 (1) (2023).
[39] S.A. Revitt-Mills, A. Robinson, Antibiotic-induced mutagenesis: under the microscope, Front. Microbiol. 11 (2020) 585175.
[40] S.S. Hawas, N.S. El-Gohary, M.T. Gabr, M.I. Shaaban, M.B. El-Ashmawy, Synthesis, molecular docking, antimicrobial, antiquorum-sensing and antiproliferative activities of new series of pyrazolo [3, 4-b] pyridine analogs, Synth. Commun. 49 (19) (2019) 2466–2487.
[41] H. Morgan, M. Lipka-Lloyd, A.J. Warren, N. Hughes, J. Holmes, N.P. Burton, E. Mahenthiralingam, B.D. Bax, A 2.8 Å structure of zoliflodacin in a DNA cleavage complex with Staphylococcus aureus DNA gyrase, Int. J. Mol. Sci. 24 (2) (2023) 1634.
[42] J.E. Deweese, N. Osheroff, The DNA cleavage reaction of topoisomerase II: wolf in sheep's clothing, Nucleic. Acids. Res. 37 (3) (2009) 738–748.
[43] A.C. Ketron, N. Osheroff, Phytochemicals as anticancer and chemopreventive topoisomerase II poisons, Phytochem. Rev. 13 (2014) 19–35.
[44] E.M. Ling, Structure and function of DNA topoisomerase II beta, Newcastle Univ., 2023.
[45] N. El-Gohary, S. Hawas, M. Gabr, M. Shaaban, M. El-Ashmawy, New series of fused pyrazolopyridines: synthesis, molecular modeling, antimicrobial, antiquorum-sensing and antitumor activities, Bioorg. Chem 92 (2019) 103109.
[46] M.K. Kathiravan, M.M. Khilare, K. Nikoomanesh, A.S. Chothe, K.S. Jain, Topoisomerase as target for antibacterial and anticancer drug discovery, J. Enzyme Inhib. Med. Chem. 28 (3) (2013) 419–435.
[47] M. Kathiresan, D. Martins, A.M. English, Respiration triggers heme transfer from cytochrome c peroxidase to catalase in yeast mitochondria, Proc. Natl. Acad. Sci. 111 (49) (2014) 17468–17473.
[48] D. Martins, M. Kathiresan, A.M. English, Cytochrome c peroxidase is a mitochondrial heme-based H2O2 sensor that modulates antioxidant defense, Free Radic. Biol. Med. 65 (2013) 541–551.
[49] W. Alam, H. Khan, M.S. Jan, H.W. Darwish, M. Daglia, A.A. Elhenawy, In vitro 5-LOX inhibitory and antioxidant potential of isoxazole derivatives, PLoS. One 19 (10) (2024) e0297398.
[50] Y.V. Karpenko, K. Medvedeva, A. Solomennyi, O. Rudenko, O. Panasenko, V. Parchenko, S. Vasyuk, Design, synthesis, molecular docking, and antioxidant properties of a series of new s-derivatives of ((1, 2, 4-triazol-3 (2H)-yl) methyl) thiopyrimidines, (2025).
[51] J.-P. Declercq, C. Evrard, A. Clippe, D. Vander Stricht, A. Bernard, B. Knoops, Crystal structure of human peroxiredoxin 5, a novel type of mammalian peroxiredoxin at 1.5 Å resolution, J. Mol. Biol 311 (4) (2001) 751–759.
[52] S. Narramore, C.E. Stevenson, A. Maxwell, D.M. Lawson, C.W. Fishwick, New insights into the binding mode of pyridine-3-carboxamide inhibitors of *E. coli* DNA gyrase, Bioorg. Med. Chem 27 (16) (2019) 3546–3550.
[53] H.J.M. Bowen, L.E. Sutton, Tables of interatomic distances and configuration in molecules and ions, Chem. Soc. (1958).
[54] F.H. Allen, O. Kennard, D.G. Watson, L. Brammer, A.G. Orpen, R. Taylor, Tables of bond lengths determined by X-ray and neutron diffraction. Part 1. Bond lengths in organic compounds, J. Chem. Soc. 2 (12) (1987) S1–S19. Perkin Transactions.
[55] S. Patai, The chemistry of the carbon-nitrogen double bond, (No Title) (1970).

[56] G.R. Desiraju, T. Steiner, The weak hydrogen bond: in structural chemistry and biology, Int. Union Cryst. (2001).
[57] G.A. Jeffrey, G.A. Jeffrey, An Introduction to Hydrogen Bonding, Oxford University Press, New York, 1997.
[58] M. Nishio, M. Hirota, Y. Umezawa, The CH/π Interaction: Evidence, Nature, and Consequences, John Wiley & Sons, 1998.
[59] P.K. Thallapally, A. Nangia, A Cambridge Structural Database analysis of the C–H··· Cl interaction: C–H··· Cl− and C–H··· Cl–M often behave as hydrogen bonds but C–H··· Cl–C is generally a van der Waals interaction, CrystEngComm. 3 (27) (2001) 114–119.
[60] P.R. Spackman, M.J. Turner, J.J. McKinnon, S.K. Wolff, D.J. Grimwood, D. Jayatilaka, M.A. Spackman, CrystalExplorer: a program for Hirshfeld surface analysis, visualization and quantitative analysis of molecular crystals, Appl. Crystallogr. 54 (3) (2021) 1006–1011.
[61] A. Baumgärtner, Shapes of flexible vesicles at constant volume, J. Chem. Phys. 98 (9) (1993) 7496–7501.
[62] N. Bogolubov Jr, F. Le Kien, A. Shumovsky, On the exactly soluble model in quantum electrodynamics, J Phys Math Gen 19 (2) (1986) 191.
[63] A. Meyer, The size of molecules, Chem. Soc. Rev. 15 (4) (1986) 449–474.
[64] S. Suda, A. Tateno, D. Nakane, T. Akitsu, Hirshfeld surface analysis for investigation of intermolecular interaction of molecular crystals, Int. J. Org. Chem. (Irvine) 13 (2) (2023) 57–85.
[65] C.F. Mackenzie, P.R. Spackman, D. Jayatilaka, M.A. Spackman, CrystalExplorer model energies and energy frameworks: extension to metal coordination compounds, organic salts, solvates and open-shell systems, IUCrJ. 4 (5) (2017) 575–587.
[66] M. Turner, J. McKinnon, S. Wolff, D. Grimwood, P. Spackman, D. Jayatilaka, M. Spackman, CrystalExplorer17, The University of Western Australia Australia, 2017.
[67] M. Canakdag, M. Feizi-Dehnayebi, S. Kundu, D. Sahin, İ.Ö. İlhan, S.K. Alhag, L. A. Al-Shuraym, S. Akkoc, Comprehensive evaluation of purine analogues: cytotoxic and antioxidant activities, enzyme inhibition, DFT insights, and molecular docking analysis, J. Mol. Struct. 1323 (2025) 140798.
[68] F. Zamiran, G.Mohammadi Ziarani, M. Feizi-Dehnayebi, M. Mirhosseyni, A. Badiei, A.M. Abu-Dief, Design, preparation, characterization, density functional theory, and HOMO-LUMO perspective of Fe3O4@ SiO2-Pr-NH-IC as a new nanomagnetic chemosensor, Appl. Organomet. Chem. 39 (2) (2025) e7998.
[69] G.Mohammadi Ziarani, M. Rezakhani, M. Feizi-Dehnayebi, S. Nikolova, Fumed-Si-Pr-Ald-Barb as a fluorescent chemosensor for the Hg2+ detection and Cr2O72− ions: a combined experimental and computational perspective, Molecules. 29 (20) (2024) 4825.
[70] M. Feizi-Dehnayebi, G.M. Ziarani, T. Lohith, S. Ghareghomi, Z. Panahande, M. Farsadrooh, M. Majidinia, Probing the biological activity of isatin derivatives against human lung cancer A549 cells: cytotoxicity, CT-DNA/BSA binding, DFT/TD-DFT, topology, ADME-tox, docking and dynamic simulations, J. Mol. Liq. 428 (2025) 127475.
[71] R. Hemmati, A. Abdi, M. Feizi-Dehnayebi, M. Farajzadeh, G.M. Ziarani, A. Banitalebi, A. Badiei, Benzoguanamine dimer as a novel fluorophore probe for Hg2+ ion detection in Pampus argenteus fish supported by DFT approach, J. Environ. Chem. Eng. (2025) 116981.
[72] N. Dehghani, G.M. Ziarani, M. Feizi-Dehnayebi, M. Mirhosseyni, A. Badiei, Synthesis and theoretical investigation of a new Hg2+ chemosensor based nanomagnetic particle (Fe3O4@ SiO2@ Pr-NCIM), Mater. Res. Bull. 183 (2025) 113200.
[73] G.Mohammadi Ziarani, D. Ebrahimi, M. Feizi-Dehnayebi, A. Badiei, A.M. Abu-Dief, Tailored silica-based sensors (SBA-Pr-Ald-MA) for efficient detection of iron (III) ions: a comprehensive theoretical and experimental viewpoint, Appl. Organomet. Chem. 39 (1) (2025) e7917.
[74] R.C. Marchi, I.A. Campos, V.T. Santana, R.M. Carlos, Chemical implications and considerations on techniques used to assess the in vitro antioxidant activity of coordination compounds, Coord. Chem. Rev. 451 (2022) 214275.
[75] J. Zhang, S. Zhang, L. Wang, W. Tan, Q. Li, Z. Guo, The antioxidant and antibacterial activities of the pyridine-4-aldehyde schiff bases grafted chloracetyl chitosan oligosaccharide derivatives, Starch-Stärke 75 (1–2) (2023) 2100268.
[76] M.S. Rana, N.M.A. Rayhan, M.S.H. Emon, M.T. Islam, K. Rathry, M.M. Hasan, M.M. I. Mansur, B.C. Srijon, M.S. Islam, A. Ray, Antioxidant activity of Schiff base ligands using the DPPH scavenging assay: an updated review, RSC. Adv. 14 (45) (2024) 33094–33123.
[77] H.S. Kareem, A. Ariffin, N. Nordin, T. Heidelberg, A. Abdul-Aziz, K.W. Kong, W. A. Yehye, Correlation of antioxidant activities with theoretical studies for new hydrazone compounds bearing a 3, 4, 5-trimethoxy benzyl moiety, Eur. J. Med. Chem. 103 (2015) 497–505.
[78] S.B. Kedare, R. Singh, Genesis and development of DPPH method of antioxidant assay, J. Food Sci. Technol. 48 (2011) 412–422.
[79] R. Apak, K. Güçlü, M. Özyürek, S.E. Çelik, Mechanism of antioxidant capacity assays and the CUPRAC (cupric ion reducing antioxidant capacity) assay, Microchim. acta 160 (2008) 413–419.
[80] J. Ceramella, D. Iacopetta, A. Catalano, F. Cirillo, R. Lappano, M.S. Sinicropi, A review on the antimicrobial activity of Schiff bases: data collection and recent studies, Antibiotics 11 (2) (2022) 191.
[81] M.A. Altamimi, A. Hussain, S. Alshehri, S.S. Imam, A. Alnami, A. Bari, Novel hemocompatible imine compounds as alternatives for antimicrobial therapy in pharmaceutical application, Processes 8 (11) (2020) 1476.
[82] A.M. Hassan, A.O. Said, B.H. Heakal, A. Younis, W.M. Aboulthana, M.F. Mady, Green synthesis, characterization, antimicrobial and anticancer screening of new metal complexes incorporating schiff base, ACS. Omega 7 (36) (2022) 32418–32431.
[83] Z. Shamsizadeh, M. Nikaeen, B. Nasr Esfahani, S.H. Mirhoseini, M. Hatamzadeh, A. Hassanzadeh, Detection of antibiotic resistant Acinetobacter baumannii in various hospital environments: potential sources for transmission of Acinetobacter infections, Env. Health Prev Med 22 (2017) 1–7.
[84] H.L. Singh, J. Singh, S. Bhanuka, Synthesis, spectroscopic characterization, biological screening, and theoretical studies of organotin (IV) complexes of semicarbazone and thiosemicarbazones derived from (2-hydroxyphenyl) (pyrrolidin-1-yl) methanone, Res. Chem. Intermed. 42 (2016) 997–1015.
[85] A.G. Erturk, Synthesis, structural identifications of bioactive two novel Schiff bases, J. Mol. Struct. 1202 (2020) 127299.
[86] F.S. Tokalı, P. Taslimi, İ.H. Demircioğlu, K. Şendil, B. Tuzun, İ. Gülçin, Novel phenolic Mannich base derivatives: synthesis, bioactivity, molecular docking, and ADME-tox studies, J. Iran. Chem. Soc. 19 (2) (2022) 563–577.